Spring 5-12-2017

SULFURIZATION OF NANOSTRUCTURED COBALT OXIDE FOR ENERGY STORAGE APPLICATIONS

Samiyah Fahad Aloqayli
Pittsburg State University, saloqayli@gus.pittstate.edu

SULFURIZATION OF NANOSTRUCTURED COBALT OXIDE FOR ENERGY STORAGE APPLICATIONS

A Thesis Submitted to the Graduate School
in Partial Fulfillment of the Requirements
for the Degree of Master of Science

Samiyah Aloqayli

Pittsburg State University

Pittsburg, Kansas

May, 2017

SULFURIZATION OF NANOSTRUCTURED COBALT OXIDE FOR ENERGY STORAGE APPLICATIONS

Samiyah Aloqayli

APPROVED:

Thesis Advisor _____
Dr. Ram Gupta, Department of Chemistry

Committee Member _____
Dr. Khamis Siam, Department of Chemistry

Committee Member _____
Dr. Pawan Kahol, Department of Physics

Committee Member _____
Dr. John Franklin, Department of English and Modern Languages

ACKNOWLEDGEMENTS

Firstly, I would like to take this opportunity to show my gratitude to several special people who have assisted me in a myriad of ways.

I would like to express my heartfelt thanks and sincere gratitude to my advisor Dr. Ram Gupta for the continuous support of my master research, for his patience, motivation, and immense knowledge. His guidance helped me in all the phases of the research and writing of this thesis. His willingness to offer me so much of his time and intellect is the major reason this thesis was completed. Thank you so much, Dr. Gupta.

Additionally, I would like to thank all my committee members: Dr. Khamis Siam, Dr. Pawan Kahol and Dr. John Franklin and all other faculty members in the Chemistry Department. Also, special thanks to Dr. Bibin Gupta and his group at NPL, India. His assistance for recording SEM and EDX images is much appreciated. Within the university, I have had the good fortune to study and work with some wonderful people: Charith K. Ranaweera and Zhuo Wang at opportune times offered me their help and wise counsel in the lab work.

To my sisters and brothers and to my best friend, Bothina, who sacrificed herself to support me to complete this thesis: I thank you all. Finally, I would like to dedicate this thesis to the memory of my mother, who first gave me roots and then wings. I miss her every day, but I am glad to know she saw this process through to its completion, offering the support to make it possible.

SULFURIZATION OF NANOSTRUCTURED COBALT OXIDE FOR ENERGY STORAGE APPLICATIONS

An Abstract of the Thesis By
Samiyah Aloqayli

Development of energy storage devices with high energy performance, power density, fast charge-discharge capability and long cyclability is needed to meet the increasing demand for energy, power and environmental protection in our daily life. Supercapacitors have great potential in future energy storage devices with magnificent properties. Recently, researchers have shown great progress for the improvement of supercapacitor performance by fabrication of nanostructured transition metal chalcogenides materials.

One of the main objectives of this thesis is to synthesize nanostructured cobalt oxide and then converte them to cobalt sulfide using a facile hydrothermal method. The synthesized cobalt oxide and cobalt sulfide were structurally and electrochemically characterized. The structural characterizations were performed using X-ray diffraction and scanning electron microscopy. The electrochemical properties were studied using a standard three-electrode cell containing a platinum wire as a counter electrode, saturated calomel electrode as a reference electrode, and synthesized materials as a working electrode. The energy storage capacity was investigated using cyclic voltammetry (CV) and galvanostatic charge-discharge techniques. Cobalt oxide and cobalt sulfide showed specific capacitances of 983 and 7358 mF/cm^2 at 2 mA/cm^2, respectively. The electrochemical properties of cobalt oxide have been improved significantly after converting to cobalt sulfide. Moreover, the effect of temperature on the electrochemical properties of the supercapacitor device fabricated using cobalt sulfide was studied. It was observed that the charge storage capacity of the device increased with increase in the temperature, which could be due to

decrease in series resistance of the device. Our results suggest that cobalt sulfide could be used as an advanced material for energy storage applications.

CONTENTS

LIST OF TABLES

LIST OF FIGURES

CHAPTER I

INTRODUCTION

Energy has become a main focus of science and of national policy as a response to growing environmental concerns. The increasing number of the technological developments around the world has caused the demand to generate different sources of energy. Since energy is the ability to do work, there's an urgent need to develop efficient and low-cost energy generation and storage devices. One of the ways to generate energy is with a conventional source such as coal and petroleum. However, there are also non-conventional sources such as solar light, hydro power, and wind energy, which are considered to be environmentally-friendly energy sources.

1.1. Different methods to generate energy:

Energy can be generated using both conventional and non-conventional ways. Non-conventional sources are environmental friendly. Solar cells, which are based on the conversion of solar light into electricity by the photovoltaic effect, have the highest efficiency and greatest number of practical applications. Solar cell technologies are divided into three generations based on materials used. The first generation of solar cells are mainly based on wafers, cells that are made of crystalline silicon. Silicon wafers are widely used due to their effective performance, as well as their high stability. The second generation is based on amorphous silicon, such as copper indium gallium selenide (CIGS) and cadmium telluride (CdTe), which are commercially significant in utility-scale photovoltaic power stations, flexible at some degree, lower in terms of material consumption, and simpler technologically to manufacture than the first generation. The third

generation is made using a variety of different organic materials such as small molecules, polymers and conductive plastics, which have low efficiency, and short stability of the absorber materials. Despite that, they are considered to be promising technologies that can achieve the goal of producing low cost and high efficiency solar cells [1].

The second common non-conventional energy source is hydro-energy, where flowing water creates energy that can be captured and turned into electricity. There are three types of hydro-energy facilities: impoundment hydroelectric, which is typically a large hydropower system; diversion hydroelectricity, which is sometimes called run-of-river, in which electricity is generated when a large proportion of a river's flow is diverted into a tunnel to power turbines before returning the water to the river further downstream; and, pumped storage hydroelectricity, which works as a battery, storing the electricity generated by other power sources [2]. Hydro-energy facilities range in size from large hydro to small hydro and micro hydro.

Wind power, another non-conventional energy source, can generate energy by converting the kinetic energy in the wind to mechanical power or electricity. There are two major types of utility-scale wind power: land-based, which is energy generated by wind turbines diffused in the ground; and offshore wind, which is similar to the standard land-based turbine, with an improvement of the conversion, which redesigns the system to be consistent with ocean conditions [3]**.** Since their efficiency has dramatically increased, they will be promising and effective ways of generating power in the future.

1.2. Most popular methods to store energy:

To have a practical application of non-conventional energy, the generated energy must be stored so that it can be available when needed. Batteries, fuel cells and capacitors are some of the most commonly used energy storage devices. Supercapacitors produce high power density with a long life cycle, and they are safer than batteries [4]. The comparisons of the power density and energy density of these devices are shown in Figure 1.1

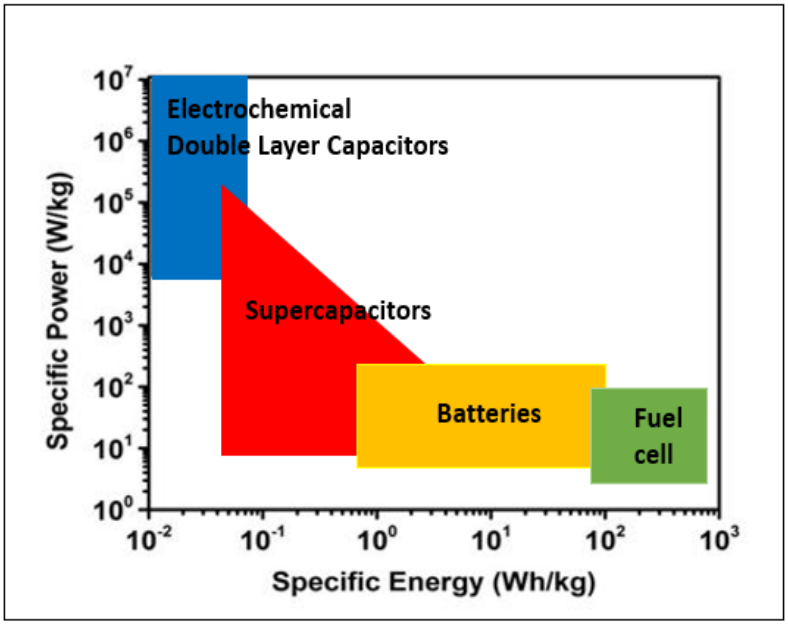

Figure 1.1: Ragone plot for various kinds of energy storage devices.

1.2.1. Batteries and capacitors:

A battery is a source of electrical energy that is provided by conversion of stored chemical energy. Batteries can be divided into two major categories: primary and secondary batteries. Primary (disposable) batteries include alkaline batteries, mercury batteries, silver-oxide batteries, and zinc-carbon batteries. Primary cells can produce current directly on assembly. Secondary batteries, which are also known as rechargeable batteries, include lead-acid batteries and lithium-ion batteries. Secondary cells are recharged by using electric current, which reverses the chemical

reactions that occur during discharge use. Generally, batteries come in many shapes and sizes from miniature cells to battery banks the size of a room [5]. Ideally, batteries should have high energy density, and should be made from environmentally friendly materials; the main problems facing various conventional batteries are slow electrode process kinetics and low-rate ionic diffusion/migration; thus, conventional batteries show huge gaps between their theoretical and practical performance [6].

On the other hand, a capacitor stores energy in the form of an electric field. The common capacitor consists of two conductive plates separated by a thin insulating material known as the dielectric as shown in Figure 1.2. The charge stored in a capacitor is proportional to the potential difference (V) between the two plates which generates an electrical field in the dielectric material

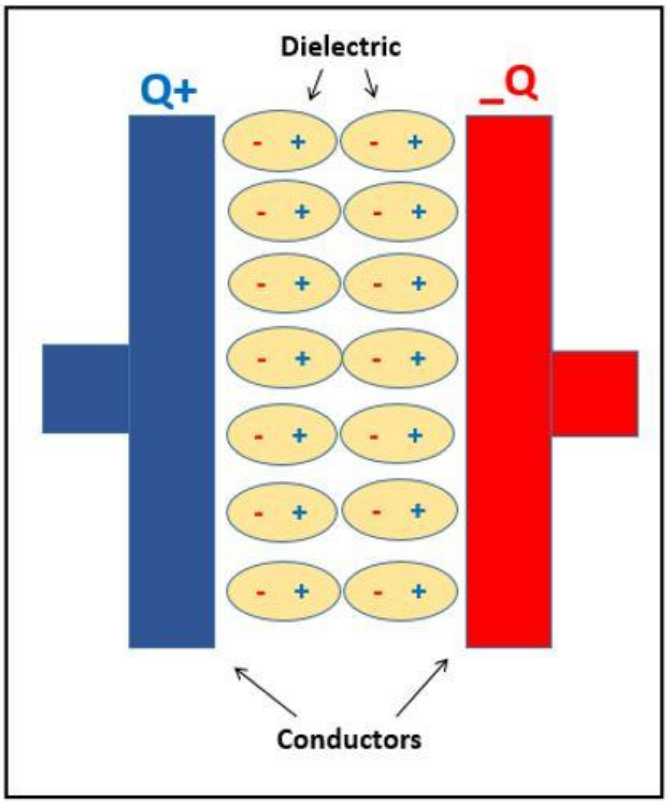

Figure 1.2: Capacitor aligns molecules of a dielectric across an electric field to store energy.

causing a charge (Q) on the both electrodes. The capacitance (C) of the device is equal to Q/V. Capacitance is measured in farads (F) [7].

A supercapacitor (SC), which is often called an ultra-capacitor or electrochemical capacitor, differs from an ordinary capacitor in terms of charging storage capacity, which is mostly higher than the storage capacity of a conventional capacitor. High power density, remarkable cyclic stability and long cycle life have been observed in supercapacitors.

Supercapacitors can be divided into three general classes: (i) electrochemical double-layer capacitors (EDLC), (ii) redox electrochemical capacitors (pseudocapacitors), and (iii) hybrid capacitors. They are, respectively, non-faradic capacitors, in which the capacitance comes from the charge separation at the electrode/electrolyte interface; faradic capacitors, in which the process occurs at the electrode interface resulting in increased capacitance; and, a combination of faradic and non-faradic capacitors. Electrical double-layer capacitors commonly use carbon-based materials, whereas pseudocapacitors use metal oxides and conducting polymers. The classification of the capacitors and most commonly used materials is shown in Figure 1.3.

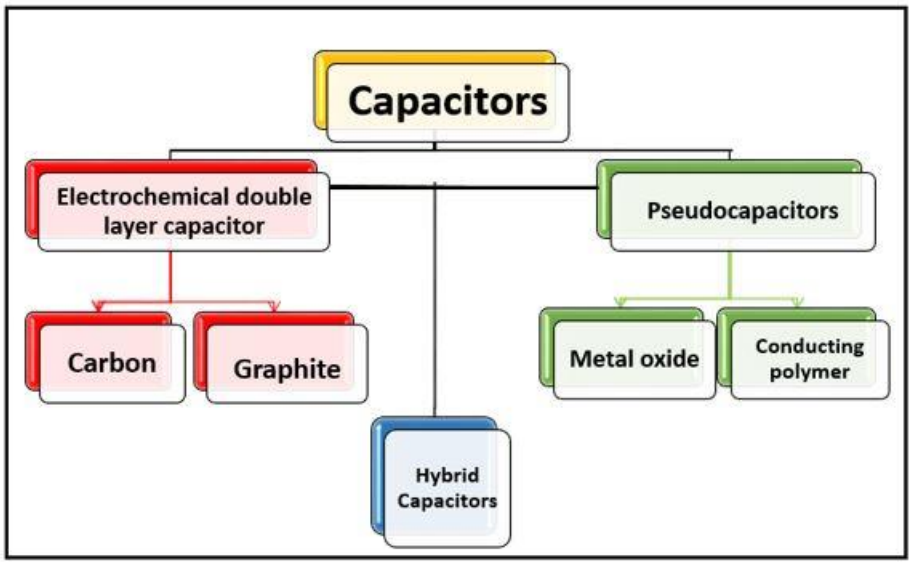

Figure 1.3: Types of capacitors and materials used.

1.2.2. Electrical double-layer capacitors:

Electrochemical double-layer capacitors are constructed from two carbon-based electrodes, an electrolyte, and a separator. EDLCs store charge electrostatically, or non-faradically, and there is no transfer of charge between electrode and electrolyte. Charge storage in EDLCs is highly reversible, which leads them to achieve high cycling stabilities. Capacitance is proportional to the surface area of the electrode, as given in the equation:

$$C = \epsilon A/d \quad \text{..... (1.1)}$$

where C is the capacitance, ϵ is the dielectric constant and d is the distance between the two electrodes. Therefore, the working electrode, which is made from carbon-based material with higher surface area, could provide high charge storage capacity [8].

The nature of the electrolyte plays a great role in the supercapacitor's design and performance. Different forms of carbon materials that can be used to store a charge in EDLC electrodes are (i) activated carbons, which are the most commonly used electrode material, and are less expensive and possess a higher surface area than other carbon-based materials; (ii) carbon aerogel, which is formed from conductive carbon nanoparticles with interspersed mesopores; and, (iii) carbon nanotubes that have high surface area, low resistance, and high stability, which allow them to be used as a stable material for an electrode in EDLC [9]. Electrical double layer capacitors can utilize different types of electrolytes: (i) aqueous electrolytes, such as sulfuric acid (H_2SO_4) and potassium hydroxide (KOH); or, (ii) organic electrolyte, such as acetonitrile. Aqueous electrolyte has low potential limit, while organic electrolyte achieved the highest energy density.

1.2.3. Pseudocapacitors:

While EDLCs charge electrostatically, pseudocapacitors charge faradically by electron charge transfer (redox process) between the electrode and electrolyte. Therefore, the faradic process

allows pseudocapacitors to achieve greater capacitance and energy densities than EDLCs. Pseudocapacitors' electrodes use mainly two materials to store a charge: conducting polymers such as polyaniline, polypyrrole, polythiophene and their related derivatives; and, metal oxides/metal sulfides [10]. Various transition-metal oxides, such as RuO_2, NiO, Fe_2O_3, Fe_3O_4, and MnO_2, are being studied for supercapacitor applications [11].

Ruthenium oxide (RuO_2) capacitance has been achieved by the insertion and removal of protons into its amorphous structure. It has been reported that ruthenium oxide is one of the most promising materials for supercapacitors due to the mixed electronic–protonic conductor [12-13]. Furthermore, the equivalent series resistance (ESR) of hydrous ruthenium oxide is lower than other materials which allow the ruthenium oxide pseudocapacitors to achieve higher energy and power densities than another conducting polymer pseudocapacitors [13].

Iron oxide (Fe_3O_4) has been studied for various supercapacitor applications. For example, Guan at al. reported specific capacitance values of 80.1 F/g, 36.1 F/g and 117.2 F/g for carbon nanotubes (CNT), Fe_3O_4 nanoparticles and CNT/Fe_3O_4, respectively, indicating that the presence of a supporting material can increase the capacitance values [14]. Mishra et al. reported that Fe_3O_4-functionalized graphenes can achieve a specific capacitance value of 180 F/g [15]. Wang et al. have used a composite of Fe_3O_4 nanoparticles grown on reduced graphene oxide (Fe_3O_4/rGO) and obtained a specific discharge capacitance of 220.1 F/g [16].

1.2.4. Hybrid Capacitors:

Hybrid capacitors are capacitors which have properties of both electrochemical double layers and pseudocapacitors. Therefore, by using both faradic and non-faradic processes to store a charge, hybrid capacitors have achieved energy, power densities and cycling stability greater than EDLCs and pseudocapacitors. The principal storage in a hybrid capacitor is configured with dissimilar electrodes, a battery-like faradic electrode and a capacitive carbonaceous electrode; it is

obligatory to optimize both electrodes by choosing a careful design [17]. Mainly, research interests have focused on three different types of hybrid capacitors distinguished by their electrode configuration: asymmetric, composite, and battery-type respectively. Since hybrid capacitors have high cell capacity, due to the large anode capacity, high reliability, high power density, and high energy density due to the electrochemical redox process at the faradic electrode, they can be used in a wide range of applications, causing a reduction in cost [18]. Wu et al. have deposited hybrid films from MnO_2 nanowires and graphene, resulting in an energy density of 30.4 Wh/kg compared to those composed of graphene/graphene with 2.8 Wh/kg, and MnO_2/MnO_2 with 5.2 Wh/kg [19]. The asymmetric hybrid MnO_2/graphene cell reported by Wu's group showed a significant superiority in energy density. After that, Fan et al. improved the energy density by incorporating MnO_2 into graphene as an electrode and complementing it to an activated carbon nanofiber-based electrode with outstanding energy density of 51.1 Wh/k [20].

Supercapacitors have some common advantages and disadvantages. One of the advantages is that the storage and release of energy does not require any chemical reactions. Also, compared to electrochemical batteries, they have unlimited and controllable cycle life. They charge and discharge very quickly and more simply than batteries, and they provide high power density. The disadvantages are that their energy density is commonly low, typically holding 1/5 to 1/10 of a battery [21].

1.3. Recent advances in materials for energy storage applications:

Since electrochemical devices have various applications in electronic devices, new improvements are required in terms of energy density, rate capability, and durability of electrodes, which clearly depend on the development of new electrode materials and electrode structures [22]. In recent years, a great deal of research has been accomplished for the improvement of supercapacitor performance by fabrication of nanostructured electrode materials such as transition metal oxides

and metal sulfides. These are important and promising electrode materials for supercapacitors due to their redox reaction that enriches energy store mechanisms, high specific capacity, which is typically 2 to 3 times higher than that of the carbon/graphite-based materials, and long cycle life [23]. Below is a literature survey for advanced materials for supercapacitor applications.

1.3.1. Cobalt oxide:

Among the transition metal oxides, Co_3O_4 is found to be one of the most important electrode materials [25]. Among important features are their higher surface area, redox properties, and controlled size and shape. Cobalt oxide has a broad range of potential applications such as electrochromic devices, heterogeneous catalysts, energy storage, active material in lithium ion batteries and solar energy absorbers [24-26-27]. Since carbon material is used as the anode material in the secondary lithium ion batteries, graphitic carbon anodes suffer from a relatively low specific capacity of (372 mA·h/g). Among potential alternatives to carbon, cobalt oxides have emerged in recent years and attracted much research effort. Cobalt oxide can be present in various phases such as CoO, Co_2O_3 and Co_3O_4; however, Co_3O_4 is the most stable cobalt oxide for LIBs [28-29].

Since size, morphology, porosity and pore size distribution of Co_3O_4 greatly affect its electrochemical performance, many researchers are attempting to fabricate it in nanoscale dimensions, such as cubic single crystals, hollow nanospheres, particles, tubes and films [25–30]. Among various synthetic routes to synthesis of Co_3O_4, hydrothermal synthesis has been shown to be a simple route for the preparation of such metal oxide nanoparticles.

Manteghi et al. studied the morphologies of nine prepared Co_3O_4 nanostructures under different temperature conditions in the presence and absence of surfactants by fabricating cobalt oxide from cobalt oxalate in the presence and absence of surfactant cetyltetramethylammonum bromide (CTAB) or Pluronic (F-127) to control the particle size [30]. They found that by using the

surfactant CTAB and F-127, and cobalt chloride in preparing cobalt oxalate precursor, the oxide particles become smaller in size. Therefore, these two structures maintain higher surface area and shorter diffusion length for electrolyte ions, which give best specific capacitance of 351 F/g and good stability over 1,000 cycles. Moreover, the Co_3O_4 coated nickel foam electrode gives high surface area with pore diameter of 17.22 nm. It was reported that similar work has been done by synthesis Co_3O_4 by (1) same salts without template having specific capacitance of 202.5 F/g ; and, by (2) $CoCl_2$ and urea without any template having specific capacitance of 280.5 F/g.

1.3.1.2. Nickel Oxide:

With high electrochemical activity, low cost, ease of process, and environmentally-friendly electrode materials, nickel oxide shows outstanding performance for lithium- ion batteries and electrochemical supercapacitors. Dar et al. studied the morphology effects on the energy storage capability of 1D NiO nanostructures [31]. By using anodized aluminum oxide (AAO) templates and oxidization of Ni nanotubes, they process 1D NiO nanostructures. Furthermore, they controlled the time and temperature of annealing to change the morphology from NiO nanotubes to NiO nanorods. Thus, after 25 min of annealing, the NTs maintained the tubular structure, and after a further 300 min of annealing time, nanorods (NRs) were formed. NiO nanotube structures give a specific capacitance of 2,093 F/g, which shows the highest ever obtained for NiO approaches the theoretical value of approximately 2,584 F/g, due to the convenient combination of high surface area and nanocrystalline grain size, while the NiO nanorod structure gave a lower a capacitance of 797 F/g. Both nanostructures give long-term stability against cyclic charging-discharging; NiO nanotubes give 125 A/g, while NiO nanorods give 80 A/g; both have no alteration to performance over 500 cycles.

Lately, Lu et al. did a series of new experiments trying to fabricate NiO nanorod arrays on Ni foam using hydrothermal method [32]. It provided a specific capacitance of 2,018 F/g with high

power density (reaching 80% of the theoretical value) as well as good cycling stability. The great performance of NiO was due to the thin rod morphology (< 20 nm), good crystallinity, well-aligned array structure and stable chemical bonding of the NiO nanorods on the Ni foam.

1.3.1.3. Nickel cobalt oxide:

Among the various metal oxides, nickel cobaltite ($NiCo_2O_4$), has become a new class of energy storage material for electrochemical supercapacitors due to low cost, low toxicity, high natural abundance, specific morphologies and structural features, and excellent electrochemical performance [35]. $NiCo_2O_4$ adopts a spinel structure in which Ni occupies the octahedral interstice and Co can take both octahedral and tetrahedral interstices [33]. Nickel cobaltite has a high degree of redox chemistry and electronic conductivity compared to the single phase of nickel and cobalt oxides. It holds at least two magnitudes higher electronic conductivity than that of NiO and Co_3O_4 [34]. Moreover, $NiCo_2O_4$ has a large power density and high energy density of up to 35 Wh/kg [35]. The synthesis of $NiCo_2O_4$ can be achieved by using one of three primary methods: (1) hydrothermal synthesis, (2) sol–gel method, and (3) electrodeposition process [35].

Since the electrochemical properties and the charge storage capacity of any electrode depends on its size and morphology, many researchers have made attempts to optimize the reaction conditions and form special morphologies for $NiCo_2O_4$ electrodes [35]. In general, 3D nanostructures have an advantage over 1D and 2D nanostructures in energy storage. For example, Chen et al. synthesized 3D hierarchical $NiCo_2O_4$ nanosheet–nanowire clusters using a facile hydrothermal method, having an ultrahigh specific capacitance of 2,000 F/g at 10 A/g, with excellent cycling stability, 93.8% retention, and high-power density of 26.1 kW k/g at a current density of 80 A/g [36]. Moreover, Zou et al. reported a facile hydrothermal synthesis for 3D $NiCo_2O_4$ micro-spheres constructed by radial chain-like $NiCo_2O_4$ nanowires with different exposed

crystal planes, having specific capacitance of 1,284 F/g with a high level of cycling stability after 3,000 cycles, and higher rate capability [37].

1.3.2. Metal sulfides:

Metal sulfides, with unique physical and chemical properties, have received a great interest as potential electrode material for energy storage applications. Metal sulfides have specific capacitance higher than metal oxides/carbon-based materials due to its rich redox chemistry, better electrical conductivity, and mechanical and thermal satiability [38 -39]. Recently, transition metal sulfides such as binary cobalt sulfides, nickel sulfides and ternary nickel cobalt sulfides, have shown great performance as supercapacitor electrode materials with a tremendous electrochemical performance [40-42].

Yang et al. used a hydrothermal method to prepare hollow CoS hexagonal nano-sheets [41]. The results showed a capacitance of 326.4 F/g and high current density in the three electrode measurements. Yang et al. synthesized flower-like NiS for supercapacitors, having high specific capacitance of 965.98 F/g [42].

1.3.2.1. Cobalt sulfide:

Cobalt sulfides have attracted extensive attention due to their remarkable physical, chemical, and electronic properties [43]. Thus, they could be used in many applications such as in catalysts, Li-ion batteries, and charge storage devices [43-44]. Cobalt sulfides are present in alternative phases such as CoS, CoS_2, Co_3S_4 and Co_9S_8.

Recently, more attention has been given to other cobalt sulfide morphologies to enhance their electrochemical performances. Hu et al. reported that the surface morphology of the cobalt sulfide depends on its phase [45]. A facile and efficient solvothermal method was used for the synthesis of cobalt sulfide CoS nanoflakes and cobalt disulfide CoS_2 nanoparticles. Thiourea and sulfur powders were used as precursors, respectively. The CoS nanoflakes showed regular

hexagonal shape, whereas CoS_2 nanoparticles showed a single-crystalline cubic structure with an average side length of 100 nm. Moreover, it was observed that the quantity of thiourea influenced the corresponding morphologies of the CoS nanostructures, but had no effect on their phase structures. Wang et al. have fabricated a 3D flower-like CoS that was used as high energy storage material [46]. This 3D flower-like CoS exhibited a high specific capacity of 850 mA h/g, which decreased to 300 mA h/g after 25 cycles.

Meng et al. have synthesized nanocomposites of 3D CoS/graphene composite hydrogel (CGH) which contain the reduced GO sheets with anchoring of CoS nanoparticles [47]. It was observed that the obtained 3D CGH have a high specific capacitance of 564 F/g at a current density of 1 A/g, with superior rate capability and high stability. The enhanced electrochemical properties were attributed to the special structure, which prevents the CoS nanoparticles from aggregating. Gu et al. have synthesized graphene-wrapped CoS nanoparticles using a solvothermal approach [48]. Results showed that CoS/graphene exhibits a high reversible capacity of 1,056 mA.h/g unique among all sulfide-based anode materials, with high cycling performances.

Unlike Meng et al., who synthesized nanocomposites of cobalt sulfide over graphene, other researchers have synthesized nanocomposites of cobalt sulfide over nickel foam. Pu et al. have successfully synthesized uniform Co_9S_8 nanotube arrays on conductive nickel foam by using a facile two-step hydrothermal method [49]. The SEM indicates that the Co_9S_8 nanotubes have a hexagonal crystal structure. The Co_9S_8 based electrode showed a specific capacitance of 1,775 F/g, with high rate capability and stable cycling performance [49]. Jana et al. prepared Co_9S_8/reduced graphene oxide (RGO) composites on nickel foam using hydrothermal reaction [50]. X-ray diffraction showed that the average crystal size of the Co_9S_8/RGO nanorods was ~25–36 nm. The electrical conductivity of the Co_9S_8/RGO composite was recorded as 1,690 S/m at room temperature, which is much higher than that of pure GO. Thus, the Co_9S_8/RGO composites coated

on nickel foam showed significant specific capacitance of 1,349 F/g with about 96% capacitance retention after 1,000 cycles.

1.3.2.2. Nickel sulfide:

Nickel sulfide, as one of the transition metal chalcogenides, has some special properties, such as paramagnetic–antiferromagnetic transition and metal insulation, and it has been used as a catalyst for hydrodenitrogenation and hydrodesulfurization reactions, a transformation toughener in window glasses, IR detectors, rechargeable lithium batteries and solar storage device [51-52]. Furthermore, nickel sulfide contains a variety of phases such as NiS, NiS_2, Ni_3S_4, and Ni_4S_3, which are electrochemically active, chemically stable, and compatible with organic solvents. Currently, researchers have been synthesizing different nickel sulfide nanostructures such as nanoparticles, nanorods, nanospheres, nanoplates flower-like architectures and urchin-like nanocrystals by different chemical solution routes [53]. Pan et al. reported the synthesis of flower- and rod-like nickel sulfide nanostructures using a green hydrothermal route [54]. The scanning electron microscopy showed that the flower-like NiS has been constructed with several nanorods with diameters of 30–160 nm. The effects of temperature and reaction time on the morphology have been also investigated. It showed that when the reaction times increased, the nanorods grew into new flakes, and the new flakes cracked and formed new nanorods with smaller diameters, while when the temperature was increased to 180 ^{o}C, the nanorods appeared with a diameter of 22 nm.

Gaikar et al. have studied the growth of interconnected nanorods/nanoplates of nickel sulfide (NiS) on titanium (Ti); an additive-free synthesis is performed by using a simple chemical bath deposition method [55]. It was observed that a NiS thin film electrode obtained high specific capacitance of 788 F/g at 1 mA/cm^2, with excellent cycling stability of 98% retention after 1,000

cycles, mostly due to the interconnected-type surface, which could provide fast electron and ion transport.

1.3.2.3. Ternary nickel cobalt sulfide:

Ternary nickel cobalt sulfide ($NiCo_2S_4$) has been considered as a promising electrode material for supercapacitors [56]. One of the advantages of $NiCo_2S_4$ is it has richer redox reactions than the corresponding binary nickel oxide and cobalt sulfide [57]. Park et al. reported that $NiCo_2S_4$ has higher conductivity than $NiCo_2O_4$, indicating that the replacement of oxygen (O) with sulfur (S) creates a more flexible structure due to sulfur's electronegativity being lower than that of oxygen, which lengthens the space between the layers, preventing the disintegration of the structure, followed by the enhancement of the electron transport efficiency in the structure [58]. However, it has disadvantages such as the difficulties of reaching its high theoretical capacitance due to the challenge in controlling the microstructures, chemical compositions, shapes, morphologies, and structural instability [59-60].

One effective way to control problems above for ($NiCo_2S_4$) is preparing a hybrid composite with highly conductive materials such as nanoporous carbons, carbon nanotubes (CNTs), and graphene sheets [56]. Li et al. prepared a novel carbon nanotubes (CNTs)/$NiCo_2S_4$ composite via a simple chemical bath deposition combined with a post-anion exchange reaction [56]. It was observed that CNTs/$NiCo_2S_4$ composites were used as a conductive network for the $NiCo_2S_4$ hexagonal nanoplates. Compared to pure $NiCo_2S_4$, they exhibited high supercapacitive performance up to 1,537 F/g, with discharge current density of 1 A/g, due to CNTs

1.4. The objective of the thesis:

The main objective of the thesis is to fabricate high performance energy storage devices which could be flexible as well as operate at high temperatures. The research was carried out in two phases: (i) the electrochemical performance evaluation of Co_3O_4 and Co_9O_8 based electrodes for

supercapacitors; and, (ii) the fabrication and testing of the device using two Co_9O_8 based electrodes. In the first phase, the synthesis of binder-free cobalt oxide on nickel substrate, which was subsequently converted to cobalt sulfide using hydrothermal method, were carried out and the Co_3O_4 and Co_9S_8 based electrodes were characterized using electrochemical and structural characterization techniques, such as Scanning Electron Microscopy (SEM); Cyclic Voltammetry (CV); and, galvanostatic charge-discharge in different electrolytes, such as 3M KOH, LiOH, and NaOH electrolytes. Based on the electrochemical studies, a further study was carried out to investigate the electrochemical properties of Co_9S_8 based electrode for supercapacitor applications. In the second phase, two Co_9S_8 based electrodes were used to fabricate a symmetrical supercapacitor device. The device's performance was studied electrochemically to validate its applicability.

CHAPTER II

EXPERIMENTAL DETAILS

2.1. Materials and synthesis:

Cobalt nitrate hexahydrate $Co(NO_3)_2 \cdot 6H_2O$ was obtained from Strem Chemicals, USA. Polyvinylpyrrolidinone (PVP), urea (CH_4N_2O), and sodium sulfide (Na_2S) were obtained from Acros Organics, USA. All the materials were used without further purification. The nickel foam that used to coat Co_3O_4 nanostructures was purchased from MTI Corporation, USA.

For the synthesis of cobalt oxides coated on Ni foam, cobalt nitrate (0.873 g), poly(vinyl pyrrolidone)(0.300 g), urea (0.722 g) and Ni foam were used. In typical synthesis, Ni foam was cleaned in 3M HCl followed by cleaning in DI water and isopropanol and acetone, respectively. Ni foam was completely dried before measuring its weight. Three millimoles of cobalt nitrate was dissolved in 8 ml of DI water/ ethanol (1:1 v/v) solution. In another beaker, 300 mg of PVP was dissolved in 10 ml DI water/ ethanol (1:1 v/v). Twelve millimoles of urea was dissolved in 18 ml DI water /ethanol (1:1 v/v) solution. After slowly adding the PVP and urea solutions to the cobalt nitrate solution, with the help of bath sonication for 10 min, the entire solution was transferred to a 45 mL Teflon line stainless steel autoclave having the pre-cleaned and weighted Ni foam and heated to 140 ^oC for 12 h. After 12 h of reaction at 140 ^oC, the reactor was cooled to room temperature naturally. The nickel foam was taken out and washed several times with distilled water and absolute ethanol. The obtained precipitate at the bottom of the Teflon container was filtered out and washed several times with deionized water. The Ni foam and the obtained powder

was dried at 60 °C for 8 h, and finally at 350 °C for 3 h. The synthesized cobalt oxide was converted to cobalt sulfide by immersing in 30 ml of 0.2M Na_2S solution. The solution was transferred into 45 ml Teflon-lined stainless steel autoclave. The reaction was carried out at 140 °C for 24 h. After cooling to room temperature naturally, the Ni foam was washed with DI water and alcohol. Ni foam was dried in vacuum at 60 °C for 6 h.

2.2. Characterizations:

The synthesized materials were characterized using a variety of techniques such as X-ray diffraction (XRD), scanning electron microscopy (SEM), and electrochemical measurements. More information of these techniques is given below:

2.2.1. X-ray diffraction:

The phase purity and structure of the prepared products were characterized by X-ray diffraction using a Shimadzu X-ray diffractometer set on the 2θ-θ scan with $CuK_{\alpha 1}$ radiation (λ=1.5406 Å) which was operating at a voltage of 40 kV with a current of 30 mA. The slits used for source and detector were 0.2 mm. Diffraction patterns in the form of X-ray counts were collected by the detector while the sample 2θ = 10° - 80°. To fulfil the geometry, an X-ray detector was placed; thus, the angle between the detector and the atomic planes was 2θ. Figure 2.1 describes the process.

2.2.2. Scanning electron microscopy:

Scanning electron microscopy uses a beam of highly energetic electrons to examine the morphology of the synthesized materials. The shape and size of the particles and morphology of the samples was studied. SEM recording was done with help from Dr. Bibin Gupta and his group at NPL, India. Schematic diagram of scanning electron microscopy is shown in Figure 2.2.

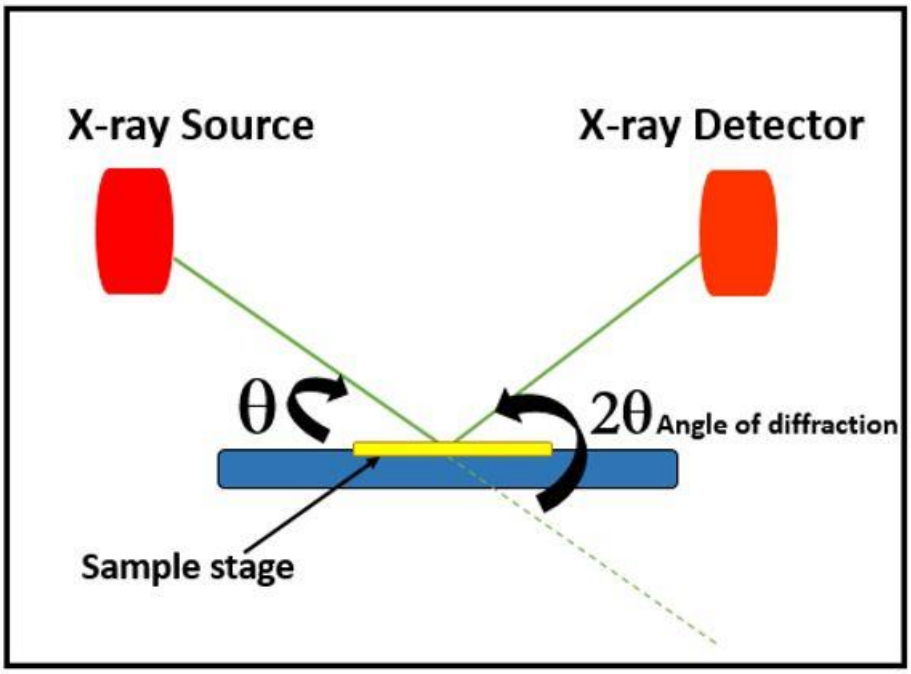

Figure 2.1: Schematic diagram of an X-ray diffractometer.

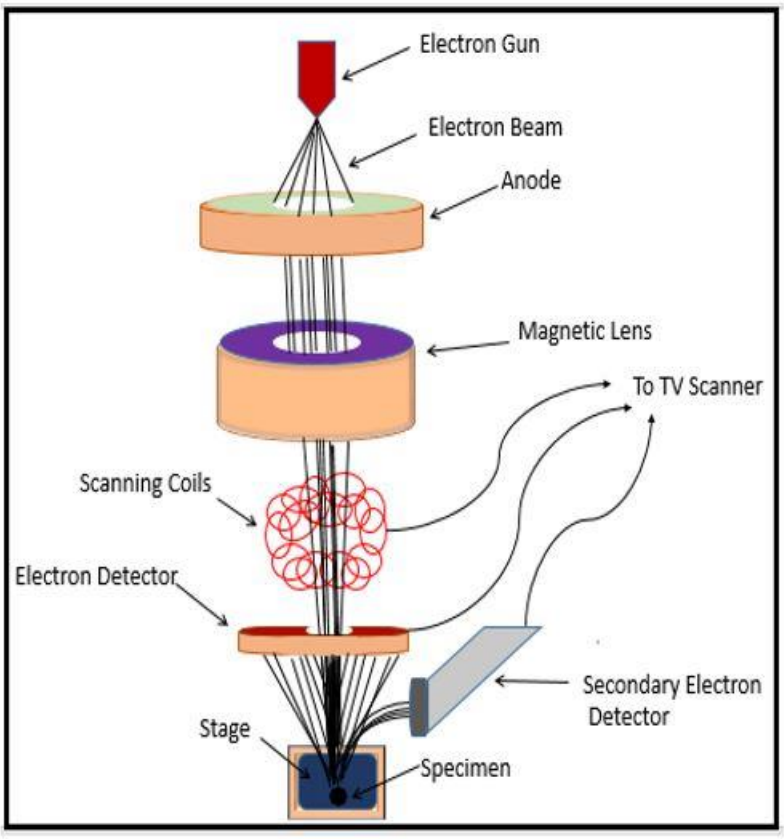

Figure2.2: Schematic diagram of scanning electron microscopy.

2.2.3. Electrochemical techniques:

The electrochemical tests were carried out in a standard three electrode cell configuration. In the three electrode measurements, cobalt oxides coated Ni foam and cobalt sulfide were used as working electrodes. A platinum wire (Pt) was used as a counter electrode, whereas the saturated calomel electrode (Hg/Hg_2Cl_2) served as the reference electrode. The schematic diagram of the three-electrode system is shown in Figure 2.3. Aqueous solutions of 3M KOH, NaOH and LiOH were used as electrolytes for these electrochemical measurements. All the electrochemical measurements were performed on a Versastat 4-500 electrochemical workstation (Princeton Applied Research, USA).

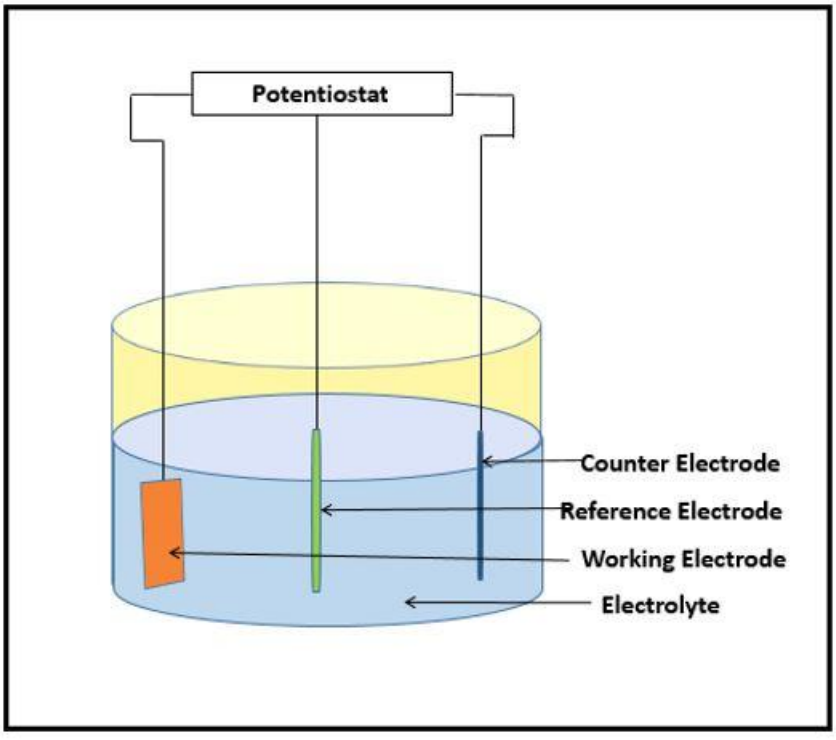

Figure 2.3: Schematic of three-cell electrochemical measurement system.

The electrochemical performance of cobalt oxide and cobalt sulfide was studied by using cyclic voltammetry (CV) and galvanostatic charge-discharge measurements. Using VersaStudio software provided by Princeton Applied Research for analyzing the giving electrochemical data, the potential applications of cobalt sulfide for electronic devices were also investigated.

A supercapacitor device was fabricated by sandwiching an ion transporting layer (Celgard, 25µm thick, 39% porosity) between two cobalt sulfide electrodes. A 3M KOH was used as an electrolyte for all the electrochemical measurements. A schematic diagram of the symmetric quasi-solid state supercapacitor is given in Figure2.4. Additionally, the electrochemical properties of cobalt sulfide performance were investigated at various temperatures (10–70 ^{o}C). The effect of temperature on the electrochemical behavior of the supercapacitor was further investigated using electrochemical impedance spectroscopy (EIS). All the electrochemical impedance measurements were performed in a frequency range of 0.05Hz to 10,000 Hz.

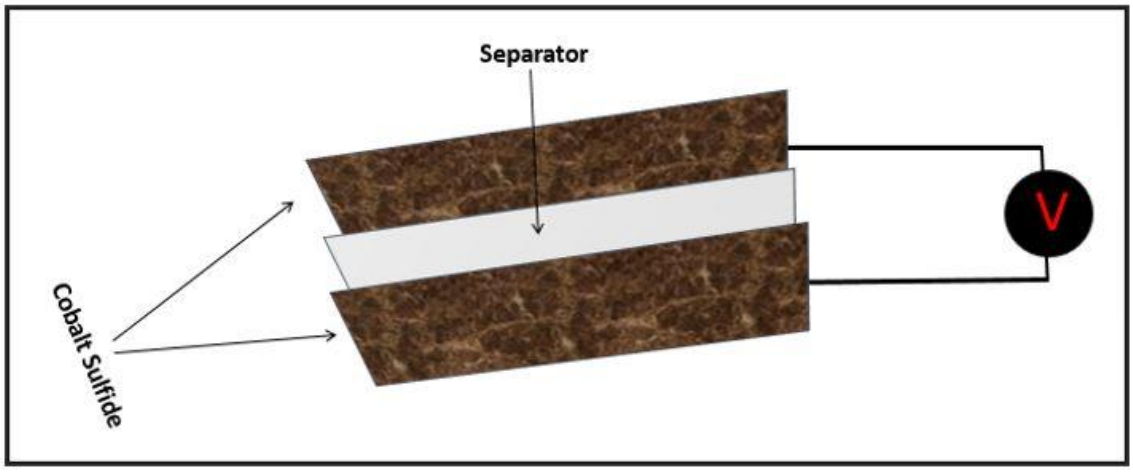

Figure 2.4: Schematic diagram of a quasi-solid state supercapacitor device.

CHAPTER III

RESULTS AND DISCUSSION

Phase purity and crystallinity of the prepared Co_3O_4 and Co_9S_8 nanostructures have been analyzed using powder X-ray diffraction. The XRD patterns of the hydrothermally synthesized Co_3O_4 over nickel foam and the converted Co_9S_8 were recorded in the two-theta range of 10-80 degrees. The pattern of Co_3O_4 shows characteristic peaks of (220), (311), (400), (511) and (440) planes, corresponding to the cubic structure of Co_3O_4. These patterns showed the intense and broad peaks suggesting highly crystalline nature of Co_3O_4 is, as shown in Figure 3.1. From synthesized Co_3O_4, that was converted to Co_9S_8 by the sulfurization process, the XRD patterns for Co_9S_8 show prominent peaks at 2θ degree values of 30.6, 36.34, 47.57 and 55.66 which are indexed respectively, as (311), (400), (511) and (600) planes of peak positions of the cubic structure of Co_9S_8, as shown in Figure 3.2. As evident from the XRD pattern, Co_9S_8 is well crystallized in nature. The two synthesized materials, Co_3O_4 and Co_9S_8, match well with standard diffraction pattern data, and the reflections can be indexed to the cubic phase of Co_3O_4 (JCPDS 42–1467) and Co_9S_8 (JCPDS 03-0631).

The XRD patterns of the cobalt oxide and cobalt sulfide were used to estimate the crystallite size of the synthesized materials. The average crystallite size (t) of all the samples was calculated using the Debye Scherrer equation [61]:

$$t = \frac{0.9\,\lambda}{\beta\,cos\theta} \quad \text{..... (3.1)}$$

Where λ is the X-ray wavelength, β is the full width at half maximum of the diffraction line, and θ is the diffraction angle of the XRD spectra. The average crystalline size of the two samples are given in Table 3.1

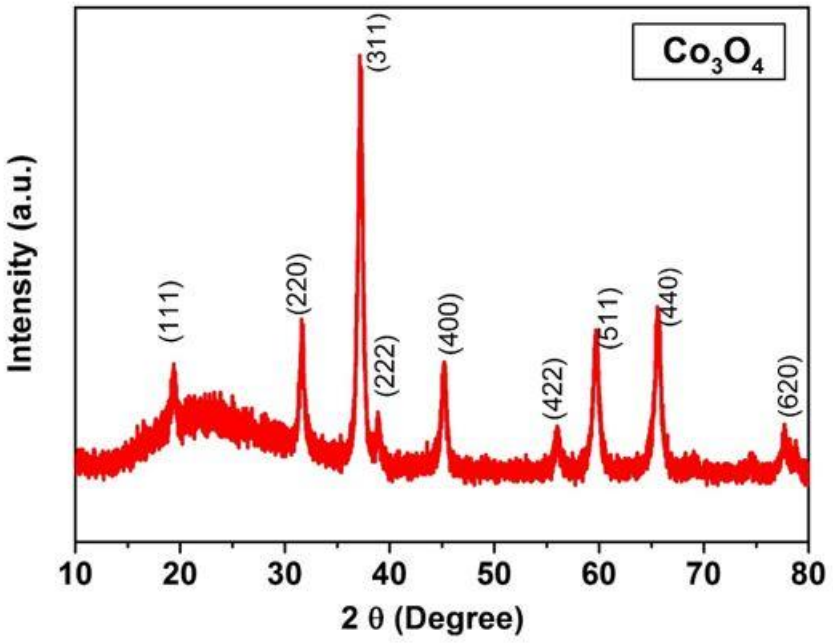

Figure 3.1: XRD patterns of Co_3O_4 nanostructures.

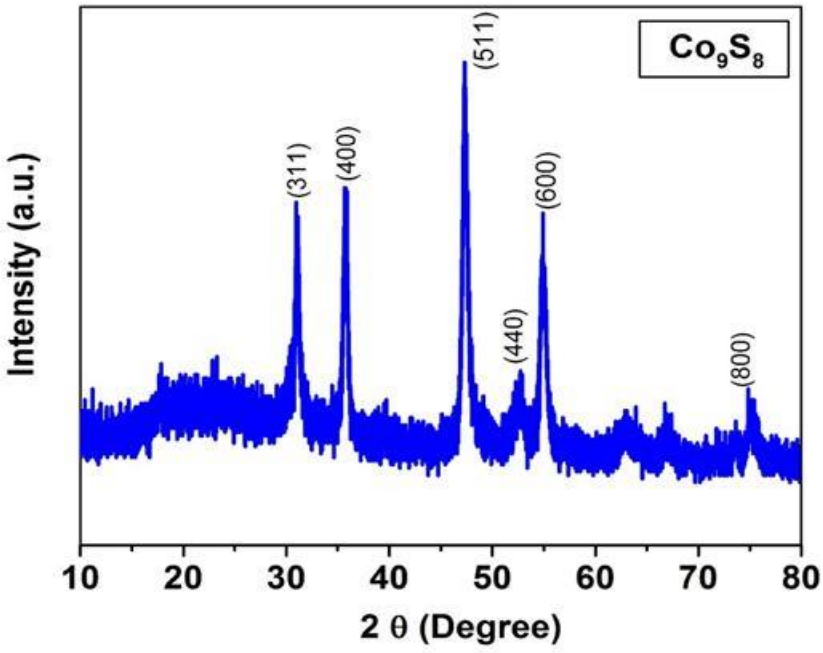

Figure 3.2: XRD patterns of Co_9S_8 nanostructures.

Table 3.1: Crystallite size of the synthesized cobalt oxide and cobalt sulfide.

Sample	FWHM (Degree)	Crystallite Size (nm)
Co_3O_4	0.0094	19.1
Co_9S_8	0.0108	17.5

3.2. Scanning electron microscopic studies:

The morphology of the synthesized Co_3O_4 and Co_9S_8 over nickel foam has been analyzed using scanning electron microscopy. The SEM images of the Co_3O_4 grown on nickel foam at various magnifications are shown in Figure 3.3. The images show flower-like morphology composed with needles, which were observed over the entire nickel foam, confirming an even deposition of cobalt oxide. The diameter of these needle-like structures is less than 10 nm with lengths of several microns. Sulfurization of these needle-like structures using a hydrothermal process convert them as nano-sheets of Co_9S_8 as shown in Figure 3.4. Elemental composition of cobalt oxide and cobalt sulfide was investigated using energy dispersive X-ray spectrometer. The EDX analysis demonstrates the presence of Co and O with atomic ratio of ~3:4 for cobalt oxide, confirming the Co_3O_4 phase. For Co_9S_8 sample, the observation of Co and S with atomic ratio of 8:9 was observed, confirming Co_9S_8 phase. The EDX patterns of the samples are shown in Figures 3.5.-3.6

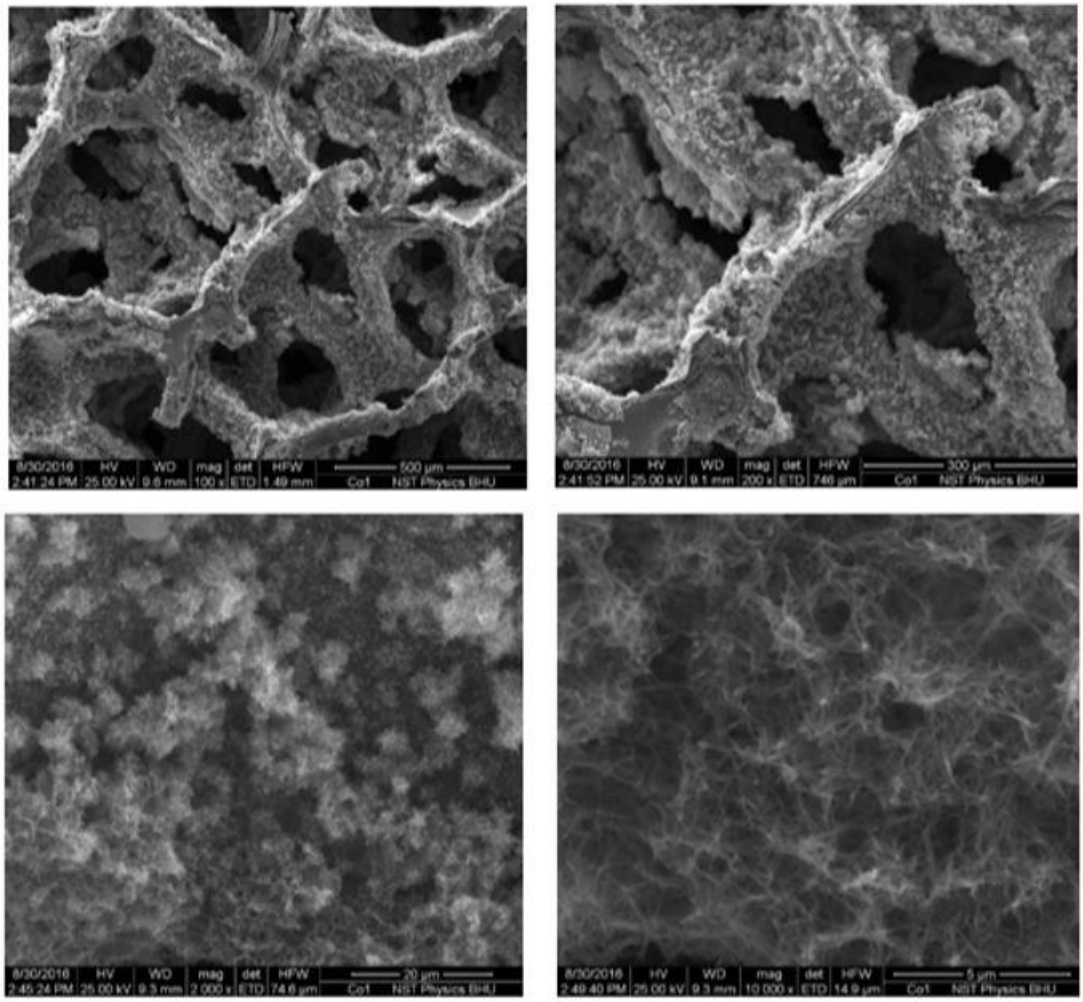

Figure 3.3: SEM images of Co_3O_4 at various magnifications.

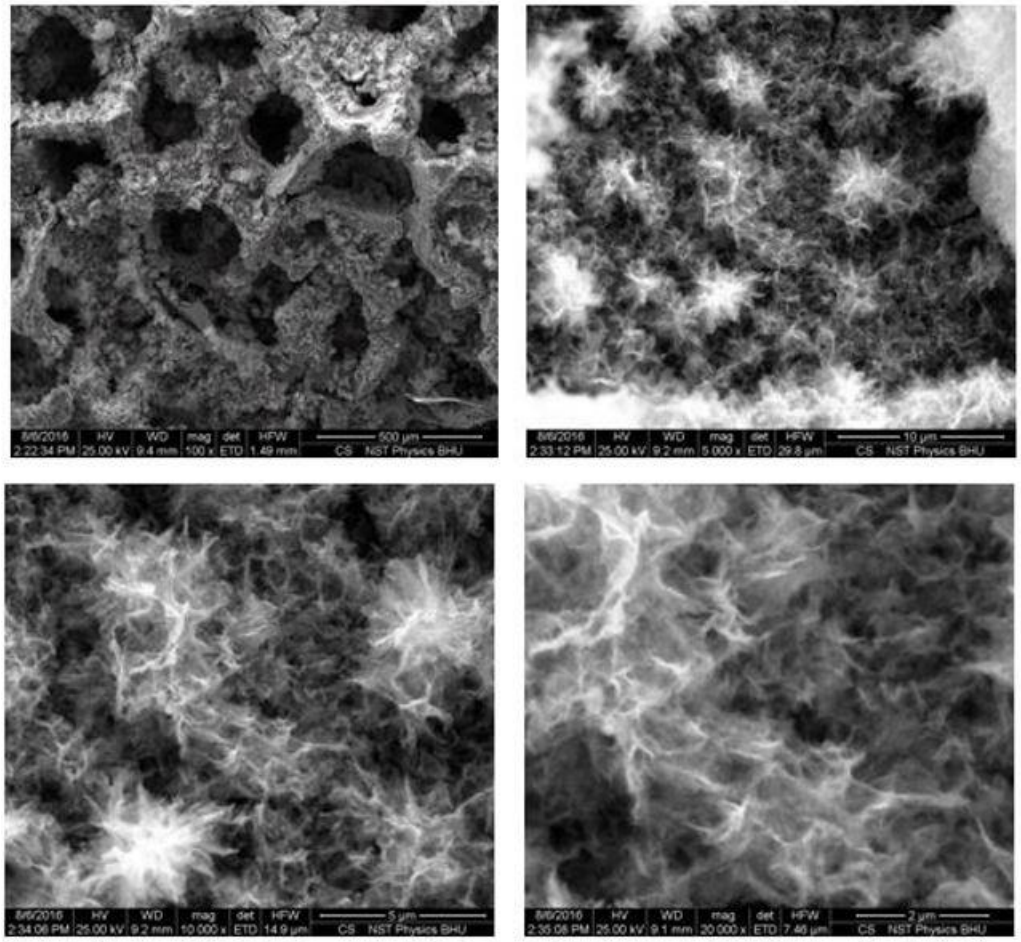

Figure 3.4: SEM images of Co_9S_8 at various magnifications.

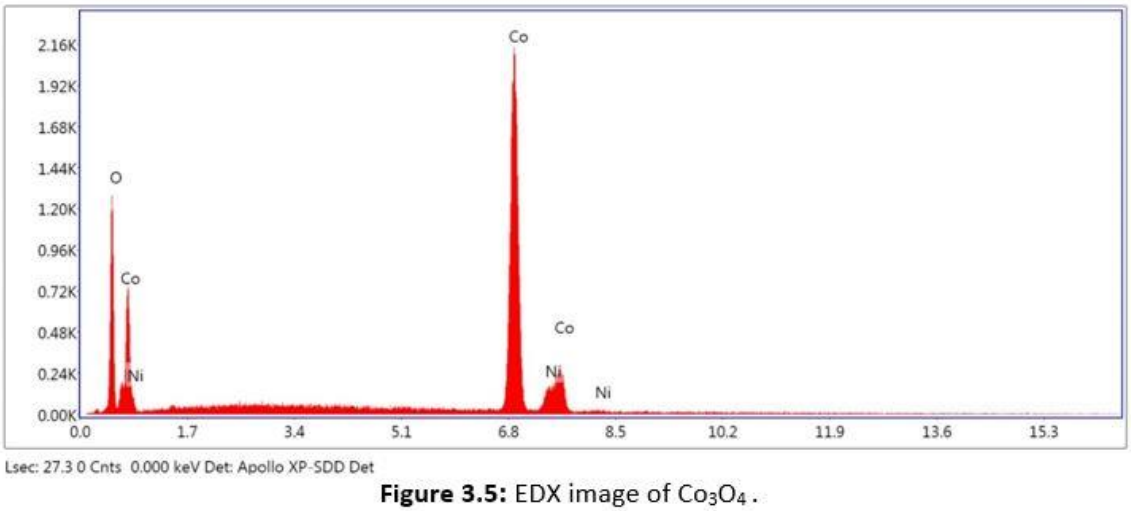

Figure 3.5: EDX image of Co_3O_4 .

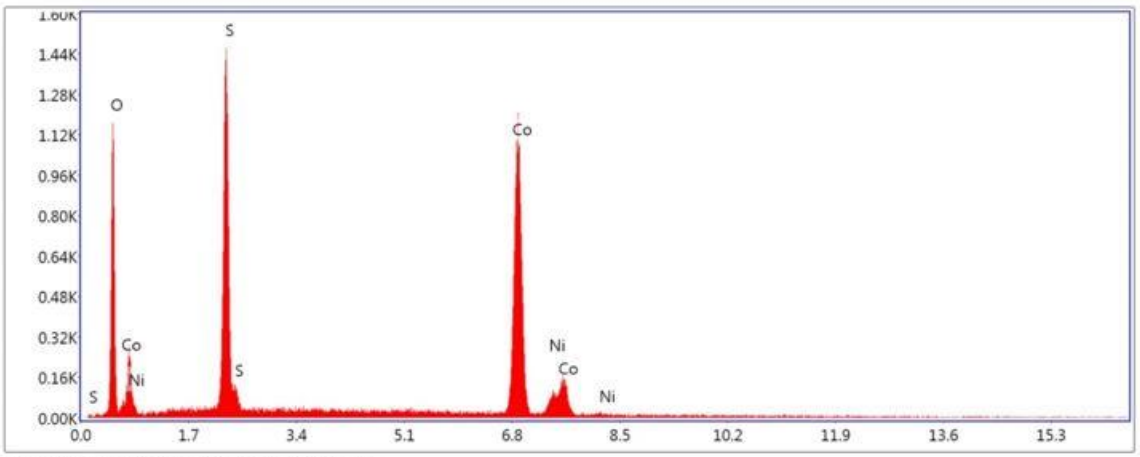

Figure 3.6: EDX image of Co_9S_8.

3.3. Electrochemical measurements:

The electrochemical performances of cobalt oxides and cobalt sulfide were systematically investigated by cyclic voltammetry and galvanostatic charge-discharge measurements. Three different electrolytes, 3M LiOH, NaOH and KOH, were used to determine the effect on the electrochemical properties of the metal oxide/sulfide. Figures 3.7-3.12 show the CV curves of the Co_3O_4 and Co_9S_8 recorded at multiple scan rates. It can be clearly observed that the shape is identical in both cobalt oxide and cobalt sulfide during the anodic and cathodic sweeps, indicating pseudocapacitance behavior of the materials. Figures 3.13-3.14 show CV curves of cobalt oxide and cobalt sulfide at low scan rates. It can be noticed that the area of the CV curves and corresponding cathodic and anodic currents improves with an increase in the scan rate, indicating that the reaction kinetics during the redox process are likely controlled by diffusion processes [66]. Two sets of redox peaks were observed in the CV curves of Co_3O_4, (peaks I/II) and (peaks III/IV) which results from reversible transition between Co_3O_4 and CoOOH and CoOOH and CoO_2. The mechanism for the redox reactions in the following equations [65]:

$$Co_3O_4 + OH^- \leftrightarrow 3CoOOH + e^- \quad \text{(I/II peaks)} \ldots\ldots\ldots\ldots \quad (3.2)$$

$$CoOOH + OH^- \leftrightarrow CoO_2 + H_2O + e^- \quad \text{(III/IV peaks)} \ldots\ldots\ldots \quad (3.3)$$

whereas, the CV curves of Co_9S_8 show one set of redox peaks, which could be due to following faradic reaction in alkaline media [67]:

$$Co_9S_8 + 9OH^- \leftrightarrow Co_9S_8(OH)_9 + 9e^- \quad \text{(I/II peaks)} \ldots\ldots\ldots \quad (3.4)$$

The specific capacitance of the cobalt oxide and cobalt sulfide electrodes was calculated by using data from cyclic voltammetric measurements [62]:

$$C_{sp} = \frac{Q}{\Delta V \times \left(\frac{\partial v}{\partial t}\right) \times A} \quad \ldots\ldots\ldots\ldots\ldots\ldots \quad (3.5)$$

Where Q is the area under the CV curve, $\partial v/\partial t$ is the scan rate, ΔV is the potential window and A is the surface area (in cm^2) of the material used such as cobalt oxide or cobalt sulfide. The variation of specific capacitance as a function of scan rate for Co_3O_4 and Co_9S_8 in different electrolytes is shown in Figures 3.15-3.22. We have determined that the highest area under the CV curve and specific capacitance in both materials was obtained from the KOH electrolyte. It was observed that the specific capacitance of the cobalt oxide electrode was decreased from 2.02 to 0.28 mF/cm^2 with an increasing scan rate from 1 mV/s to 200 mV/s, and decreased in the specific capacitance of cobalt sulfide from 14.77 to 0.55 mF/cm^2 with increasing scan rate from 1 mV/s to 200 mV/s, respectively, which could be due to an insufficient time for the electrochemical reactions to occur at each electrode. At a higher scan rate, the concentration of the ions at the electrode/electrolyte interface increases rapidly and the diffusion rate of electrolyte from electrode/electrolyte interface to electrode will not be enough to satisfy the electrochemical reactions [64].

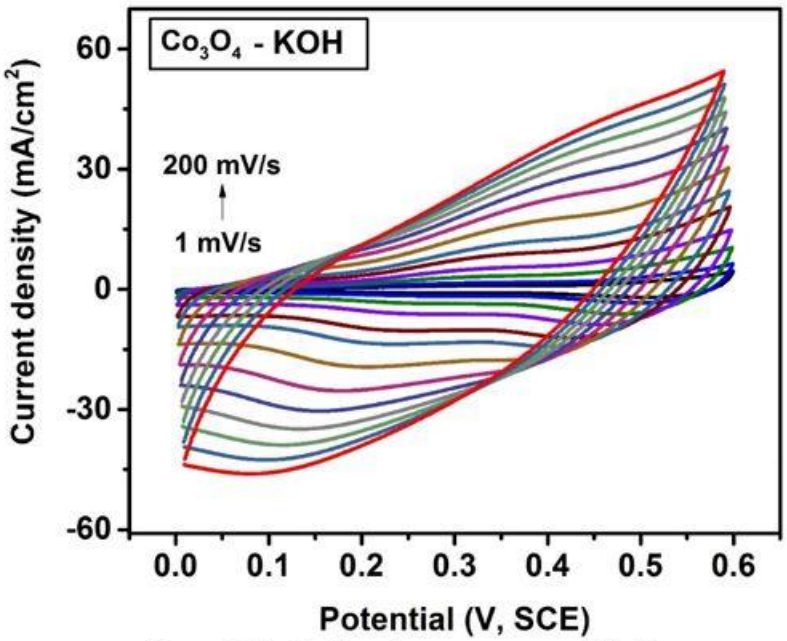

Figure 3.7: Cyclic voltammograms of Co_3O_4 at various scan rates in 3M KOH electrolyte.

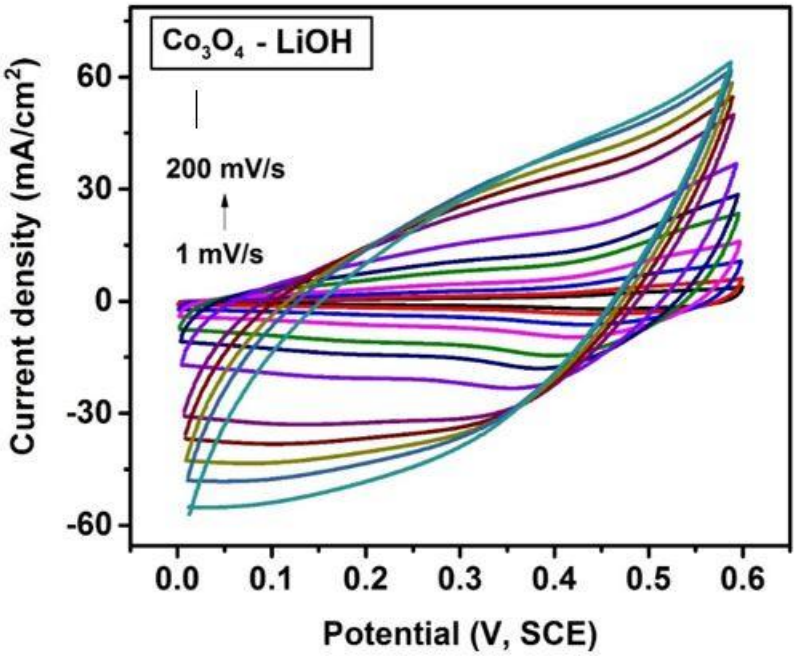

Figure 3.8: Cyclic voltammograms of Co_3O_4 at various scan rates in 3M LiOH electrolyte.

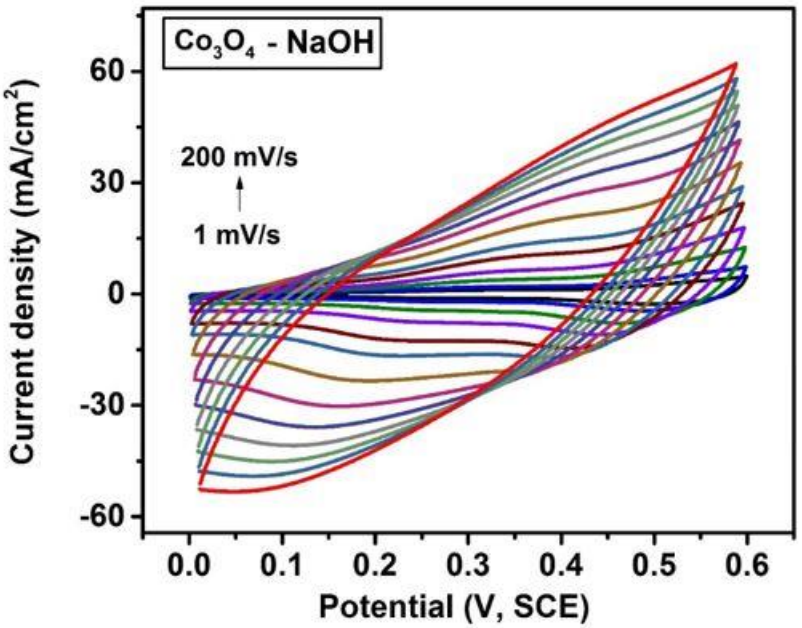

Figure 3.9: Cyclic voltammograms of Co_3O_4 at various scan rates in 3M NaOH electrolyte.

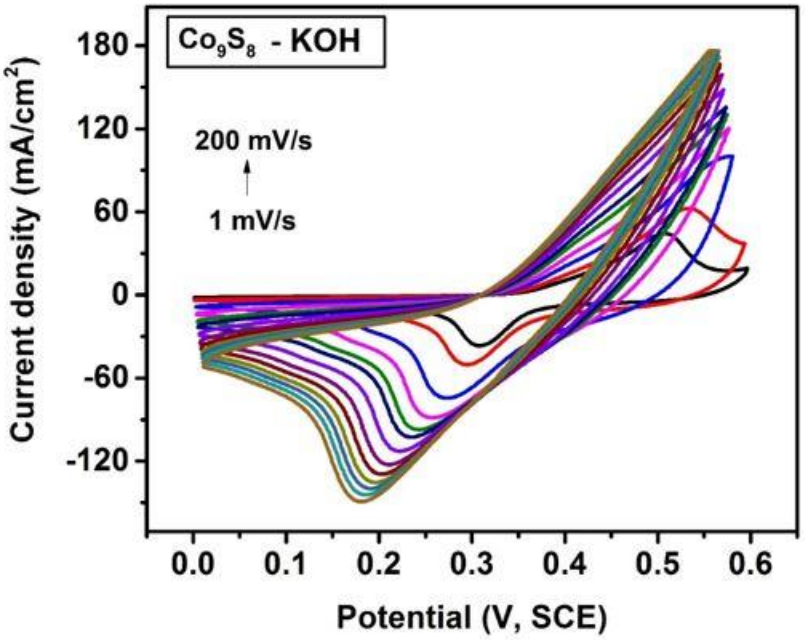

Figure 3.10: Cyclic voltammograms of Co_9S_8 at various scan rates in 3M KOH electrolyte.

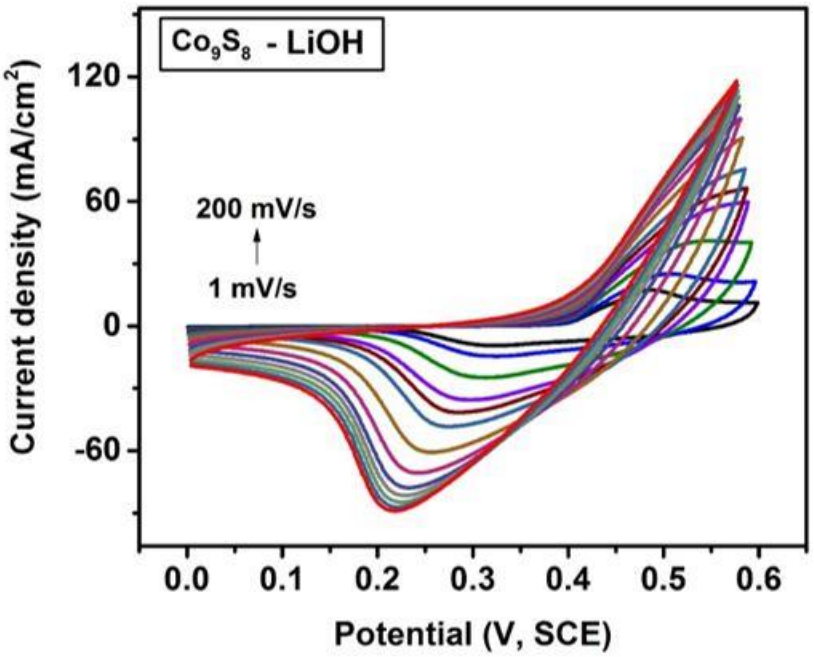

Figure 3.11: Cyclic voltammograms of Co_9S_8 at various scan rates in 3M LiOH electrolyte.

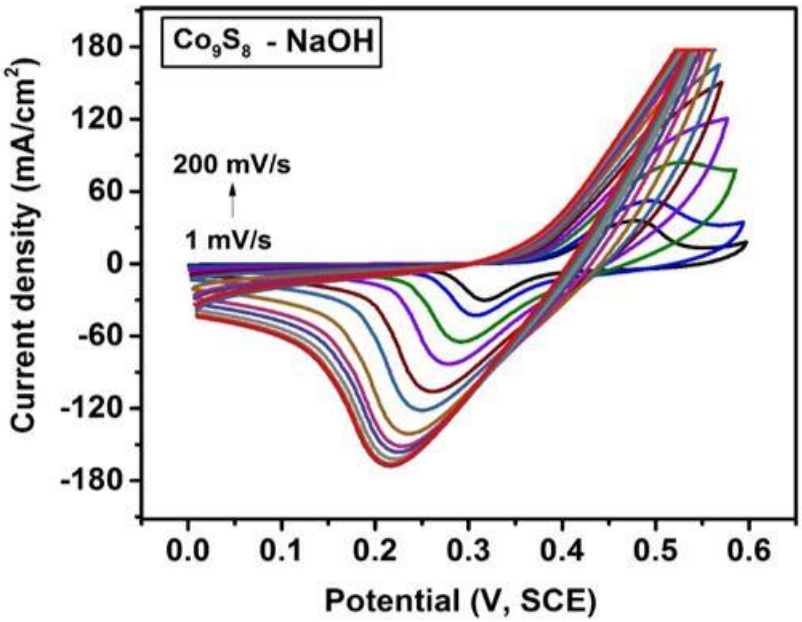

Figure 3.12: Cyclic voltammograms of Co_9S_8 at various scan rates in 3M NaOH electrolyte.

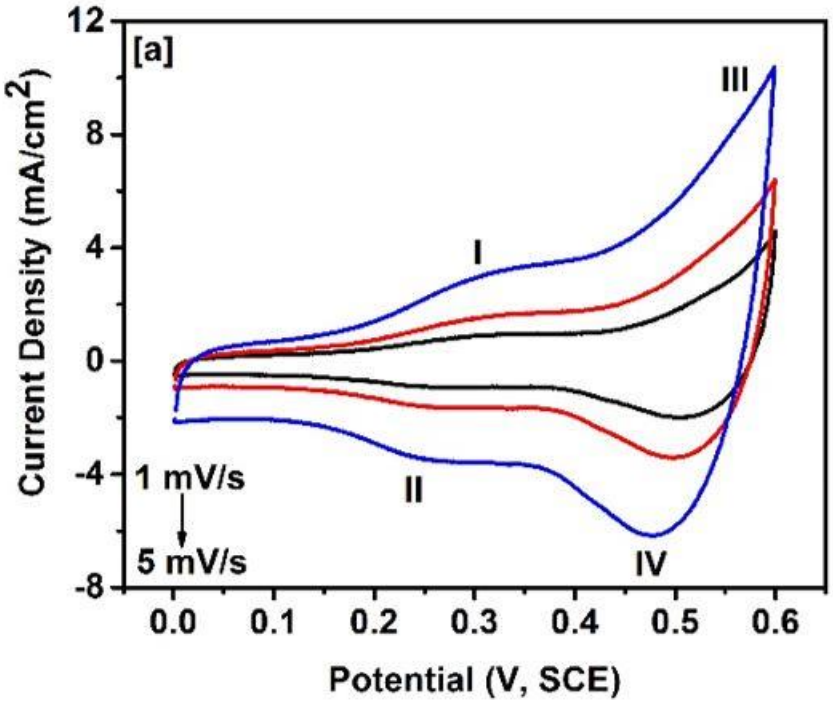

Figure 3.13: Cyclic voltammograms of Co_3O_4 at low scan rates in 3M KOH electrolyte.

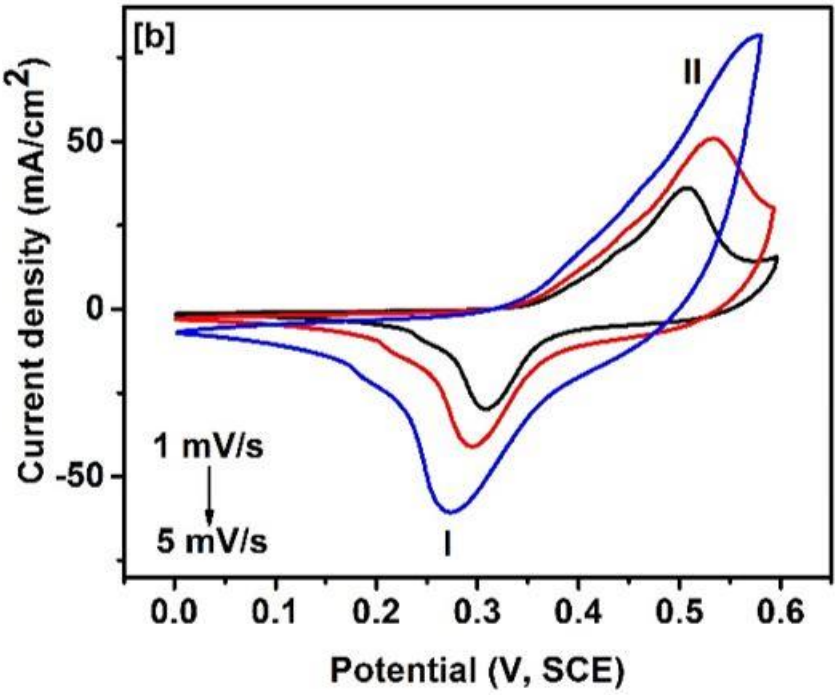

Figure 3.14: Cyclic voltammograms of Co_9S_8 at low scan rates in 3M KOH electrolyte.

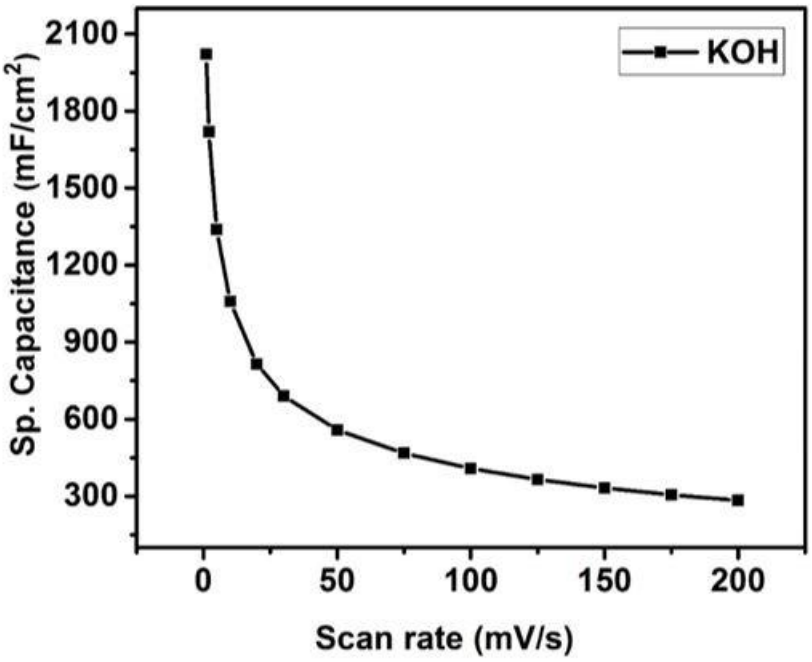

Figure 3.15: Variation of specific capacitance as a function of scan rate for Co_3O_4 in 3M KOH electrolyte.

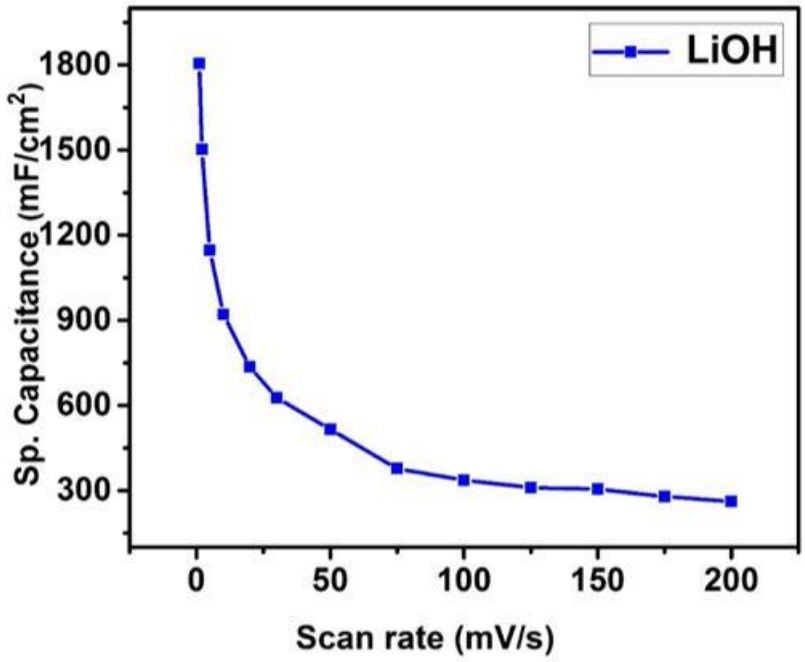

Figure 3.16: Variation of specific capacitance as a function of scan rate for Co_3O_4 in 3M LiOH electrolyte.

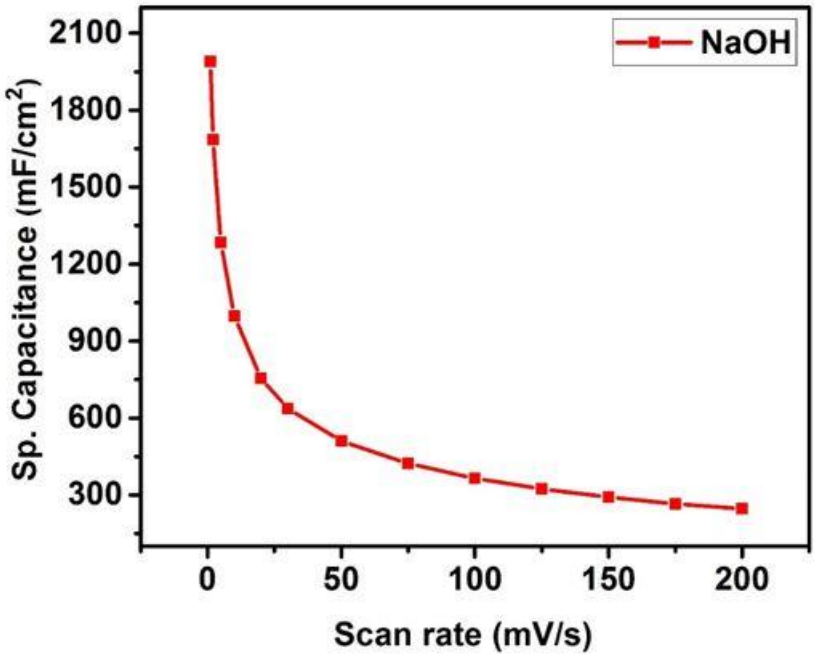

Figure 3.17: Variation of specific capacitance as a function of scan rate for Co_3O_4 in 3M NaOH electrolyte.

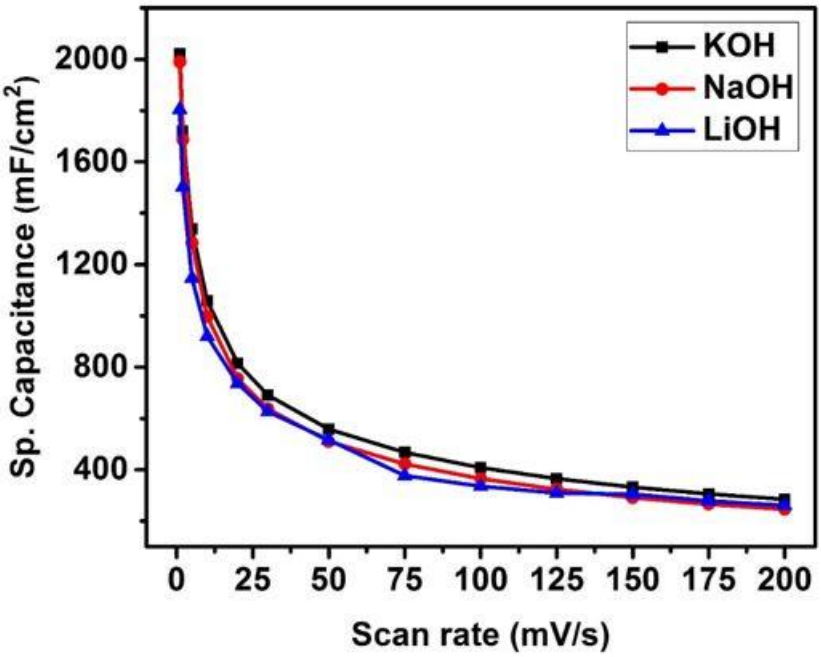

Figure 3.18: Variation of specific capacitance as a function of scan rate for sample Co_3O_4 in different electrolytes.

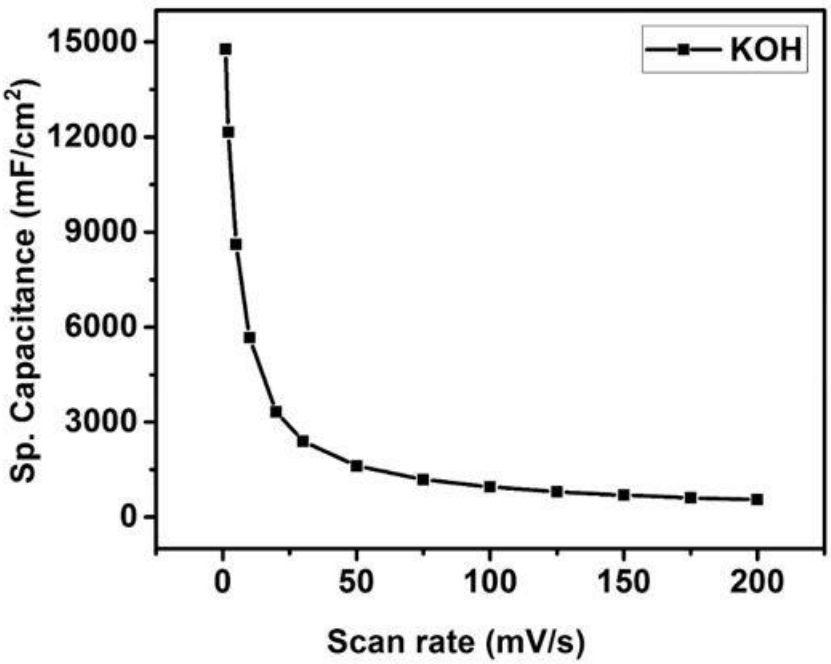

Figure 3.19: Variation of specific capacitance as a function of scan rate for Co_9S_8 in 3M KOH electrolyte.

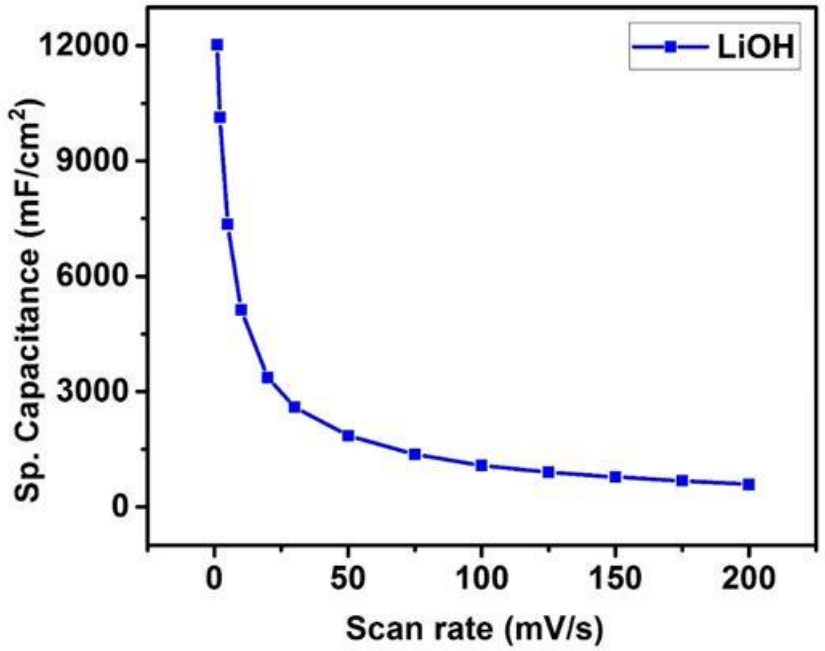

Figure 3.20: Variation of specific capacitance as a function of scan rate for Co_9S_8 in 3M LiOH electrolyte.

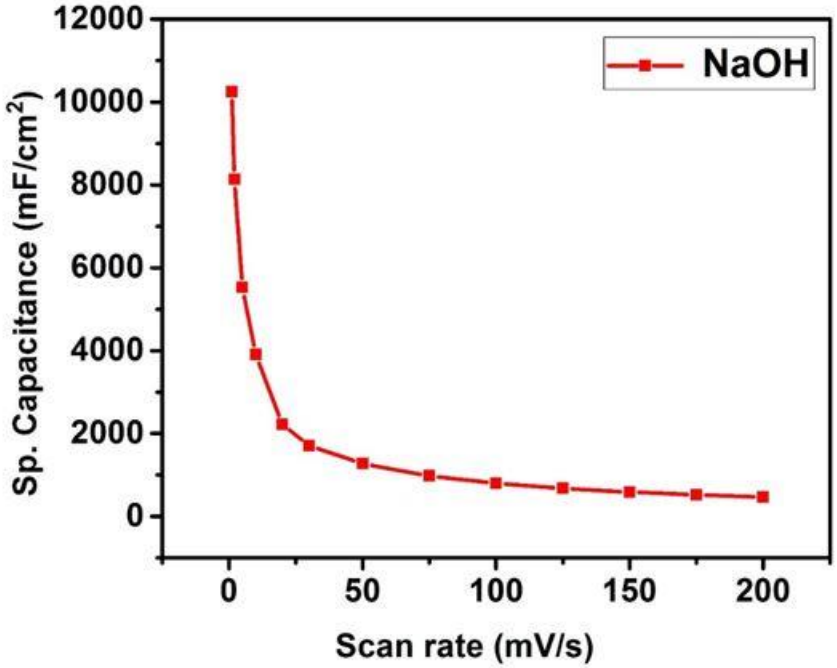

Figure 3.21: Variation of specific capacitance as a function of scan rate for Co_9S_8 in 3M NaOH electrolyte.

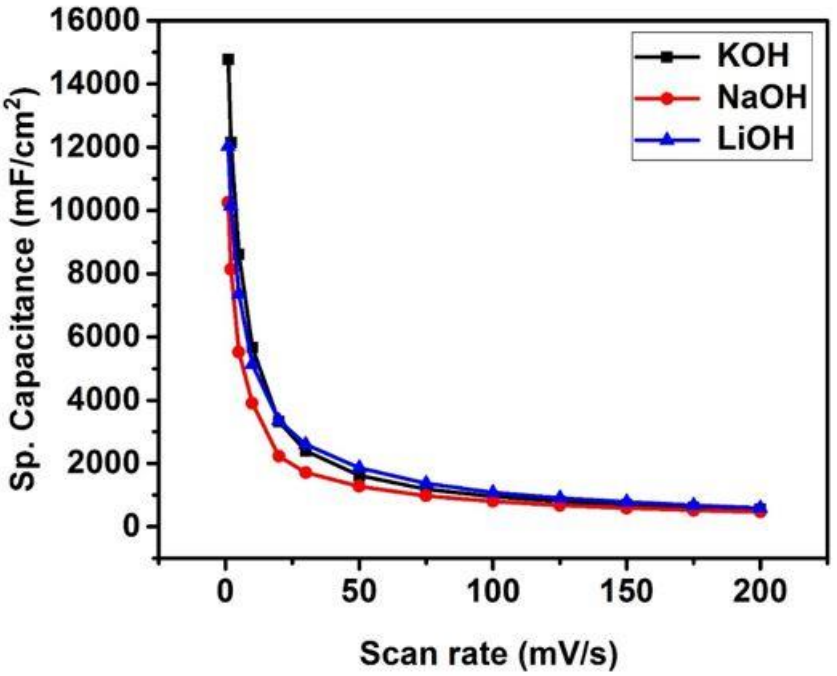

Figure 3.22: Variation of specific capacitance as a function of scan rate for Co_9S_8 in different electrolytes.

The charge storage capacity of the Co_3O_4 and Co_9S_8 electrodes for supercapacitors was further investigated using galvanostatic charge-discharge measurements. These measurements were performed in three different electrolytes, 3M LiOH, NaOH and KOH, in the potential range of 0 to 0.6V (*vs.* SCE). The charge-discharge study was performed at various discharge current densities. The charge-discharge characteristics of the cobalt oxide and cobalt sulfide electrodes are shown in Figures 3.23-3.28. The discharge curves were observed to be decreased when the current increased due to the faradic reactions and fast reaction kinetics of cobalt oxide and cobalt sulfide electrodes [63]. A potential platform was observed in charge-discharge curves, which indicates that the electrode was behaving as a typical pseudocapacitor. This might refer to the charge transfer reaction or to the electrochemical adsorption/desorption process at the electrode/electrolyte interface. Moreover, the charge time was increased after sulfurization of Co_3O_4 suggesting improved charge storage capacity. The specific capacitance of cobalt and cobalt sulfide, 983 and 7358 mF/cm^2 at 2 mA/cm^2, respectively. The specific capacitance (C_{sp}) of the electrode materials was calculated using the equation given below [11]:

$$C_{sp} = \frac{I \times \Delta t}{\Delta V \times A} \qquad \text{..... (3.6)}$$

Where I is the discharge current (A), Δt is the discharge time (s), ΔV is the potential window (V), and A is the surface area of the cobalt oxide and cobalt sulfide. Figures 3.29-3.36 show the variation of specific capacitance versus discharge current for the cobalt oxide and cobalt sulfide electrodes, respectively, in various electrolytes. As seen, the specific capacitance of Co_3O_4 and Co_9S_8 nanostructures decreased when discharge current was increased. This could be due to an increase in potential drop and insufficient faradic redox reaction at higher current density [11].

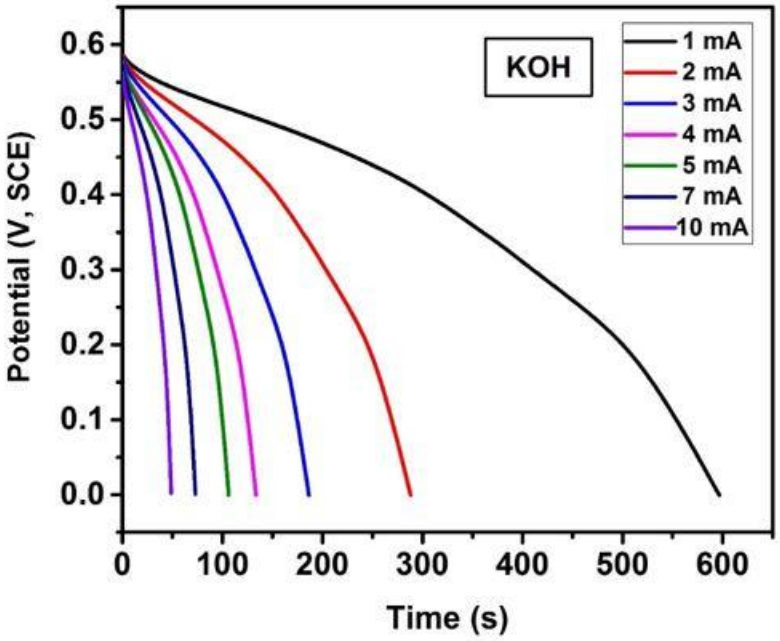

Figure 3.23: Galvanostatic charge-discharge characteristics of Co_3O_4 at various applied currents in 3M KOH electrolyte.

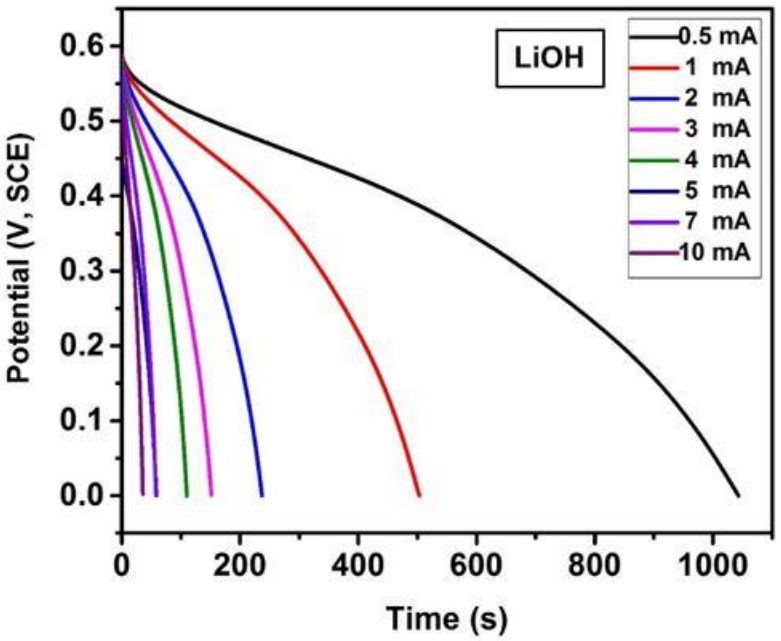

Figure 3.24: Galvanostatic charge-discharge characteristics of Co_3O_4 at various applied currents in 3M LiOH electrolyte.

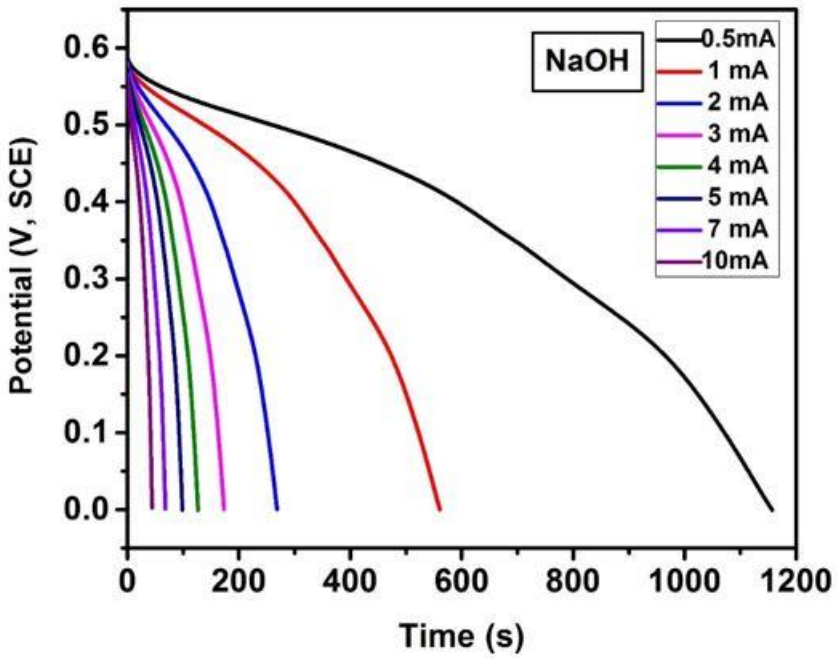

Figure 3.25: Galvanostatic charge-discharge characteristics of Co_3O_4 at various applied currents in 3M NaOH electrolyte.

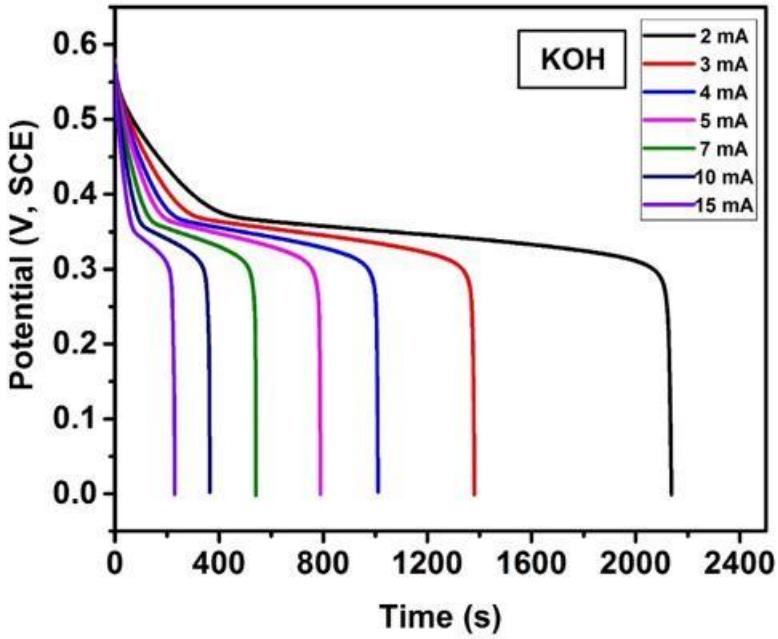

Figure 3.26: Galvanostatic charge-discharge characteristics of Co_9S_8 at various applied currents in 3M KOH electrolyte.

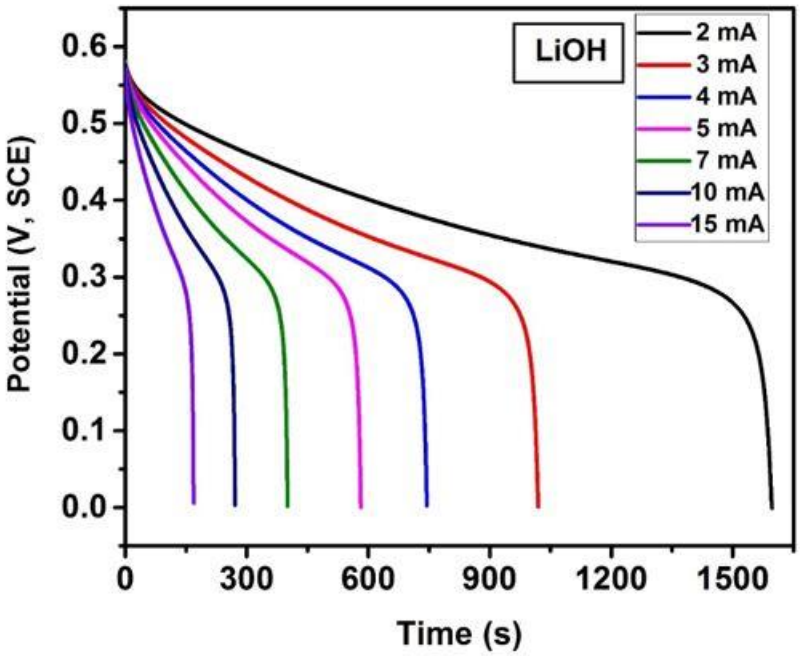

Figure 3.27: Galvanostatic charge-discharge characteristics of Co_9S_8 at various applied currents in 3M LiOH electrolyte.

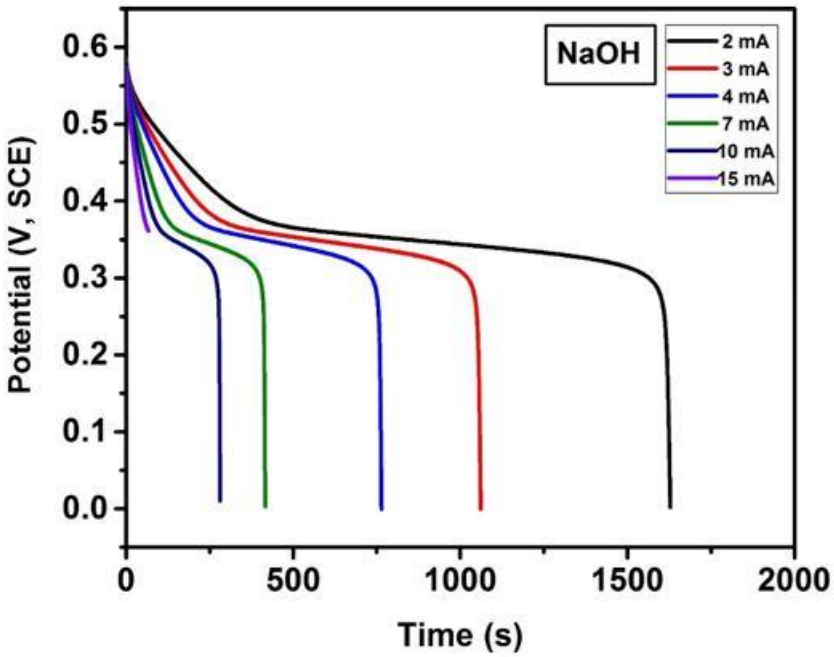

Figure 3.28: Galvanostatic charge-discharge characteristics of Co_9S_8 at various applied currents in 3M NaOH electrolyte.

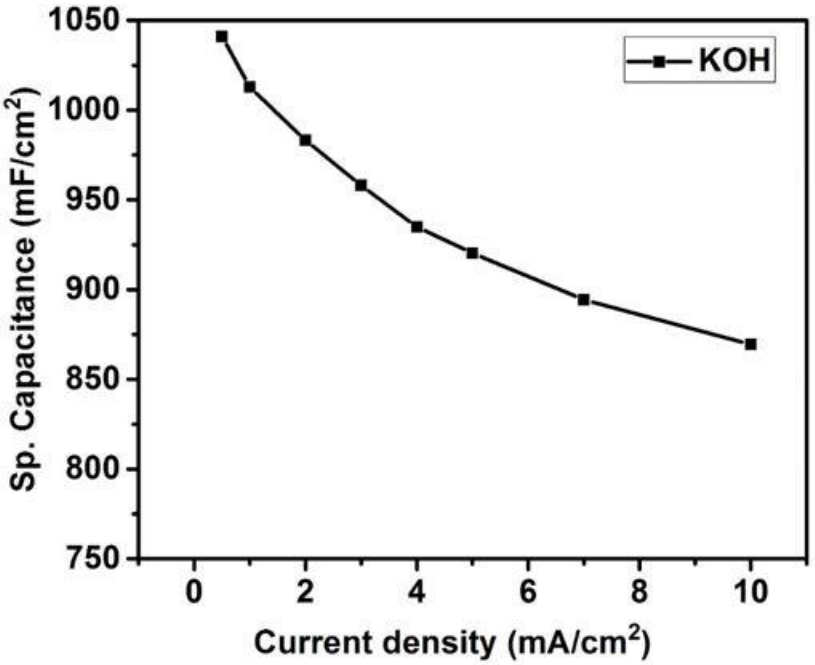

Figure 3.29: Variation of specific capacitance with applied current in 3M KOH electrolyte for Co_3O_4.

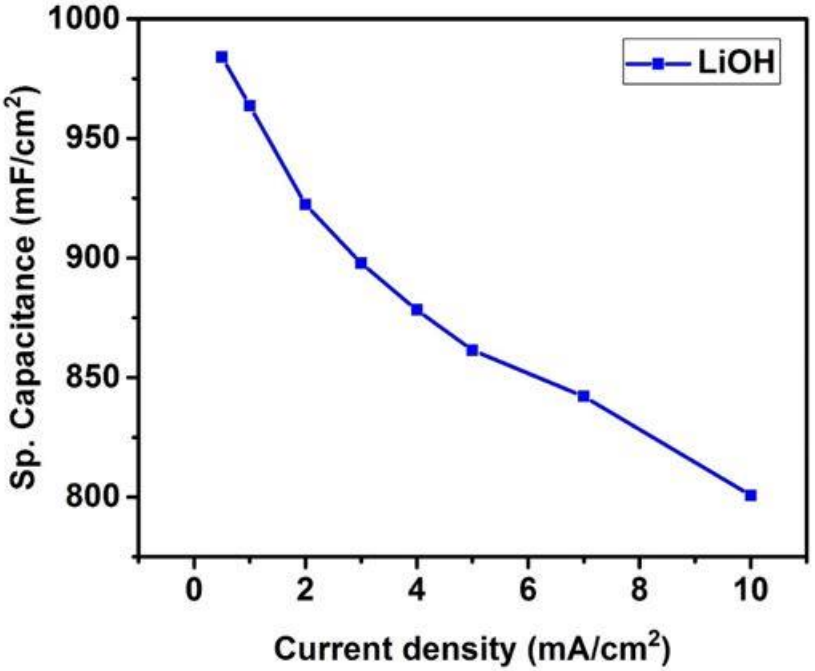

Figure 3.30: Variation of specific capacitance with applied current in 3M LiOH electrolyte for Co_3O_4.

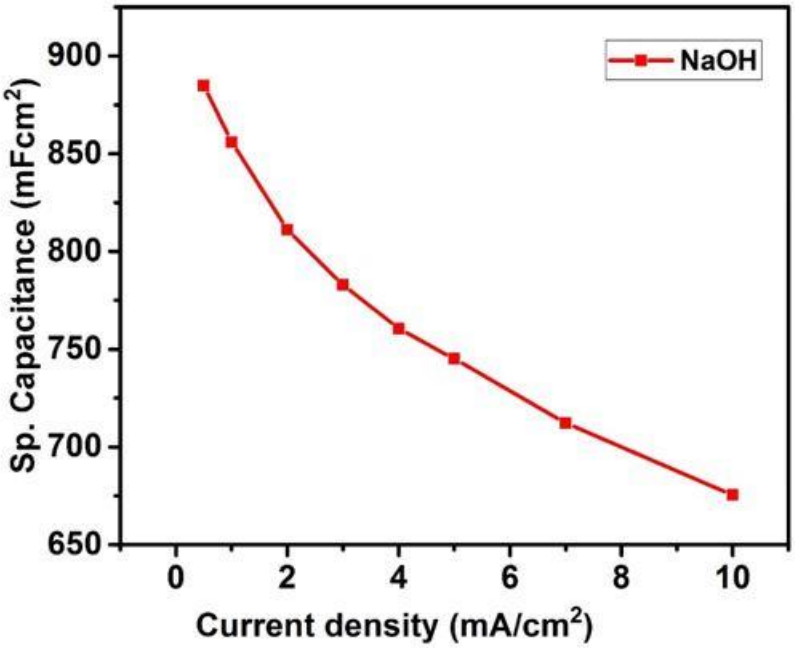

Figure 3.31: Variation of specific capacitance with applied current in 3M NaOH electrolyte for Co_3O_4.

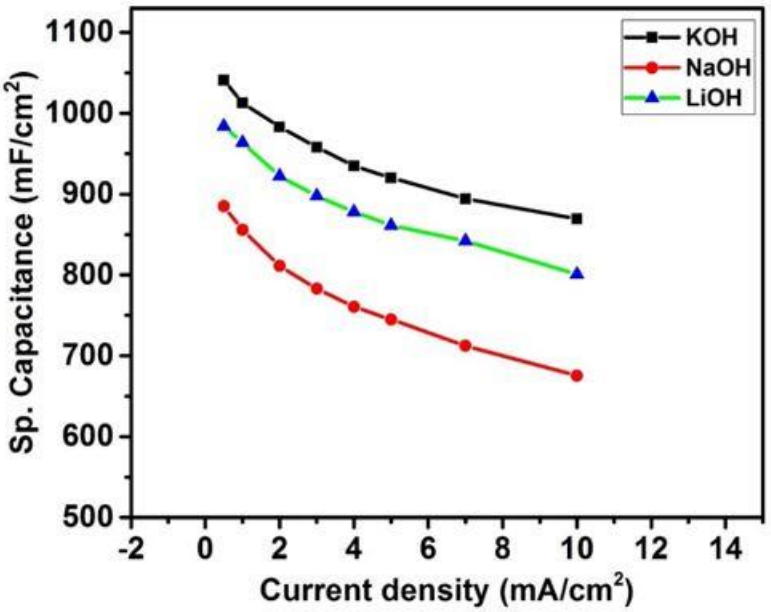

Figure 3.32: Variation of specific capacitance with applied current in different electrolytes for Co_3O_4.

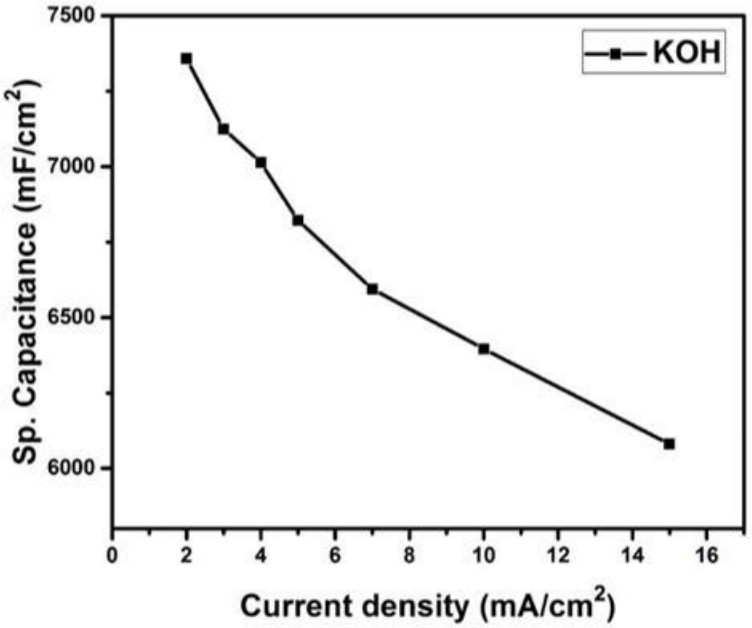

Figure 3.33: Variation of specific capacitance with applied current in 3M KOH electrolyte for Co_9S_8.

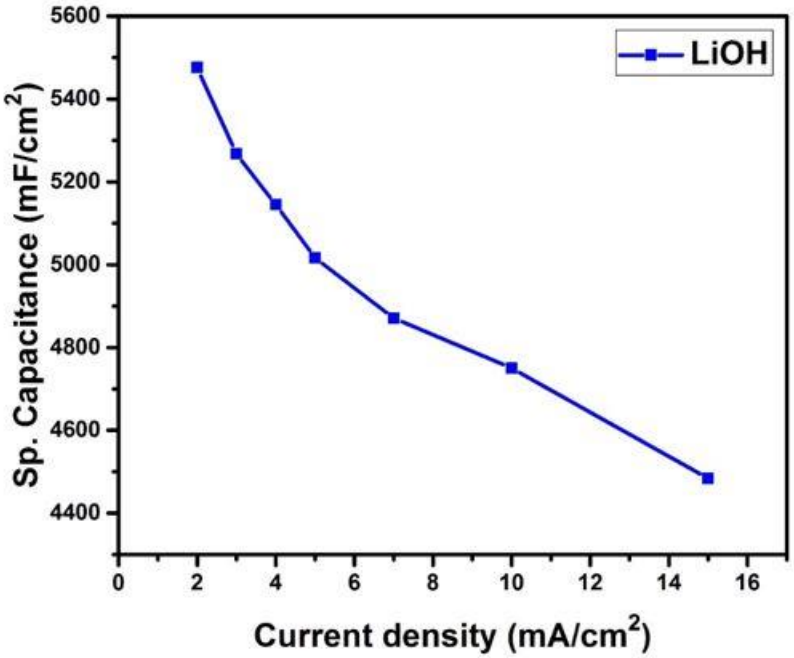

Figure 3.34: Variation of specific capacitance with applied current in 3M LiOH electrolyte for Co_9S_8.

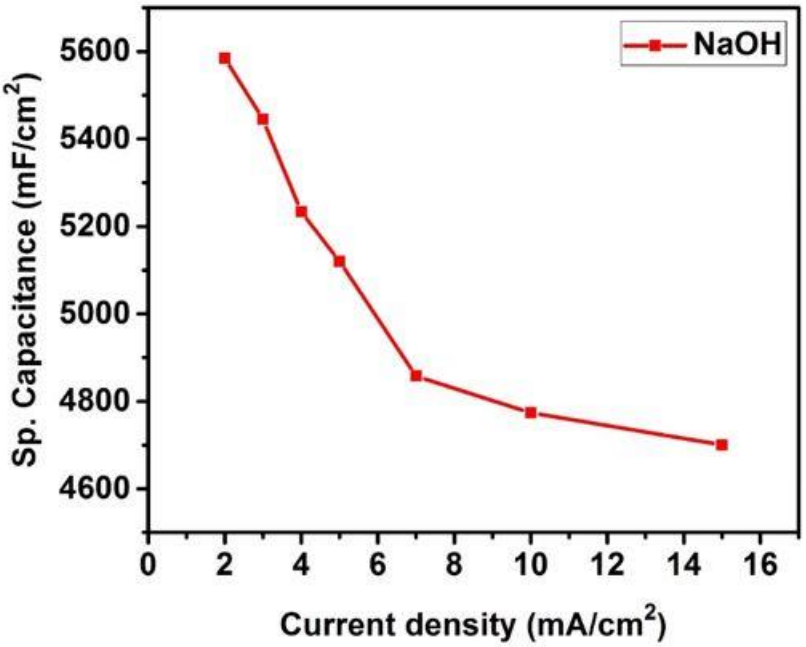

Figure 3.35: Variation of specific capacitance with applied current in 3M NaOH electrolyte for Co_9S_8 .

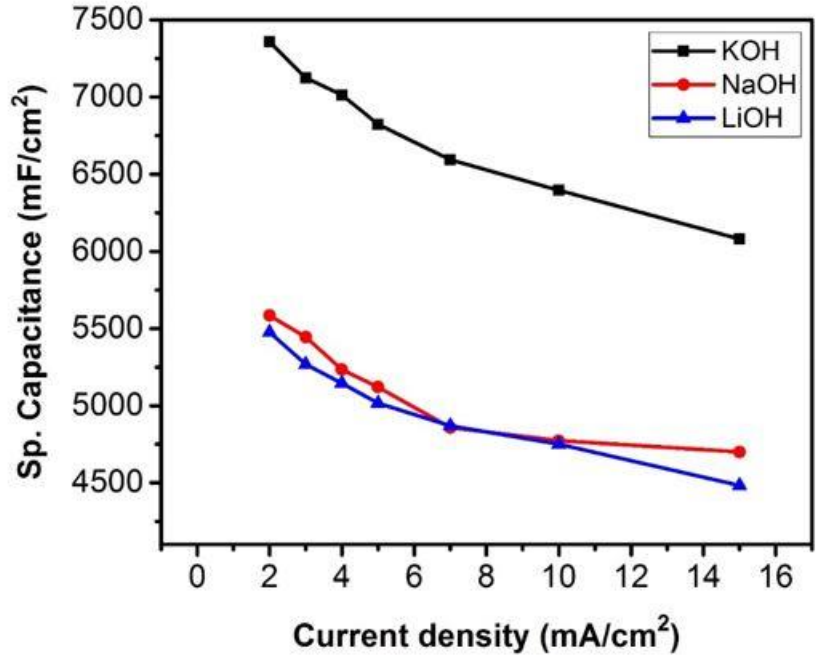

Figure 3.36: Variation of specific capacitance with applied current in different electrolytes for Co_9S_8 .

The energy density and the power density of the cobalt oxide and cobalt sulfide nanostructures were calculated to examine the performance of the supercapacitors using the expressions below [63]:

$$E\left(\frac{Wh}{cm^2}\right) = \frac{C_{sp} \times \Delta V^2}{7.2} \qquad \text{..... (3.7)}$$

$$p\left(\frac{W}{cm^2}\right) = \frac{E \times 3600}{t} \qquad \text{..... (3.8)}$$

Where C_{sp} (mF/cm^2) is the specific capacitance calculated from charge-discharge characteristics, ΔV (V) is the potential window and t (s) is the discharge time. Figures 3.37-3.44 show variations of power density versus energy density (Ragone plot) for cobalt oxide and cobalt sulfide electrodes in 3M KOH, LiOH and NaOH electrolytes. It was observed from these figures that the higher energy density corresponds to the lower discharge currents. On the contrary, power density is higher for the higher discharge currents. The highest specific capacitance for Co_3O_4 (983 mF/cm^2), specific energy density (0.038 Wh/kg), and power density (2.80 W/kg) was observed for the KOH electrolyte, and the highest specific capacitance for Co_9S_8 (7,358 mF/cm^2), specific energy density (0.27 Wh/kg), and power density (4.24W/kg) was observed for the KOH electrolyte. Furthermore, the high values of power density and energy density observed in the cobalt sulfide electrode suggest that this material could be used for high performance energy storage devices.

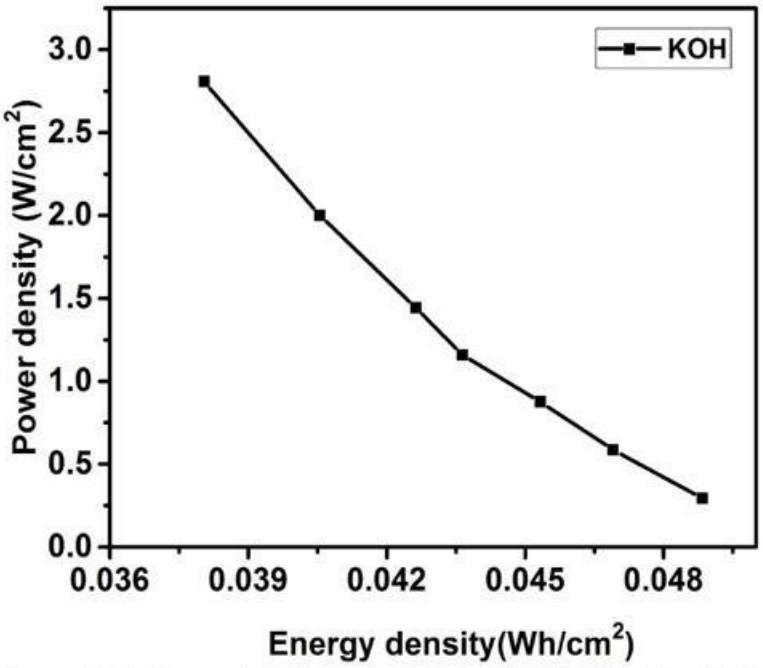

Figure 3.37: Power density versus energy density plots for Co_3O_4 in 3M KOH electrolyte.

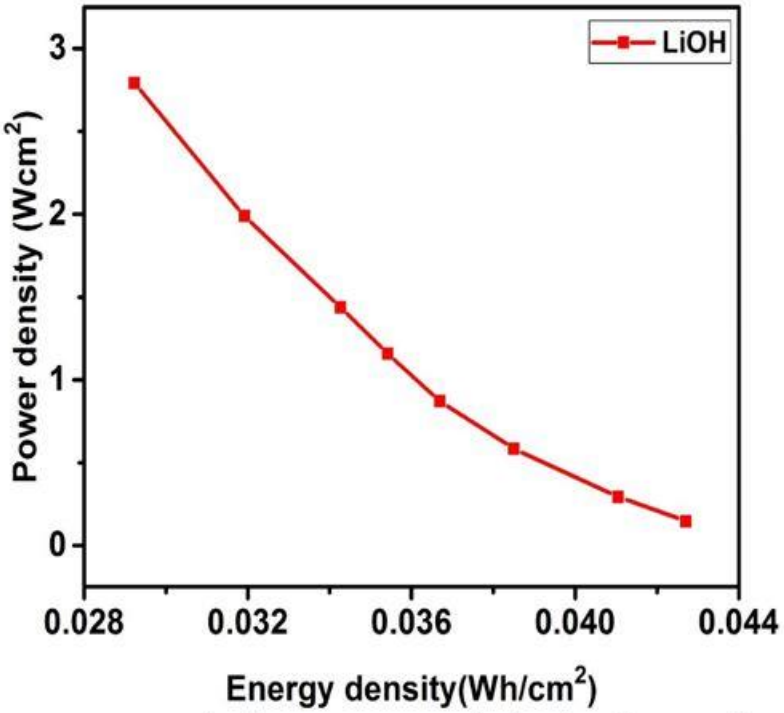

Figure 3.38: Power density versus energy density plots for Co_3O_4 in 3M LiOH electrolyte.

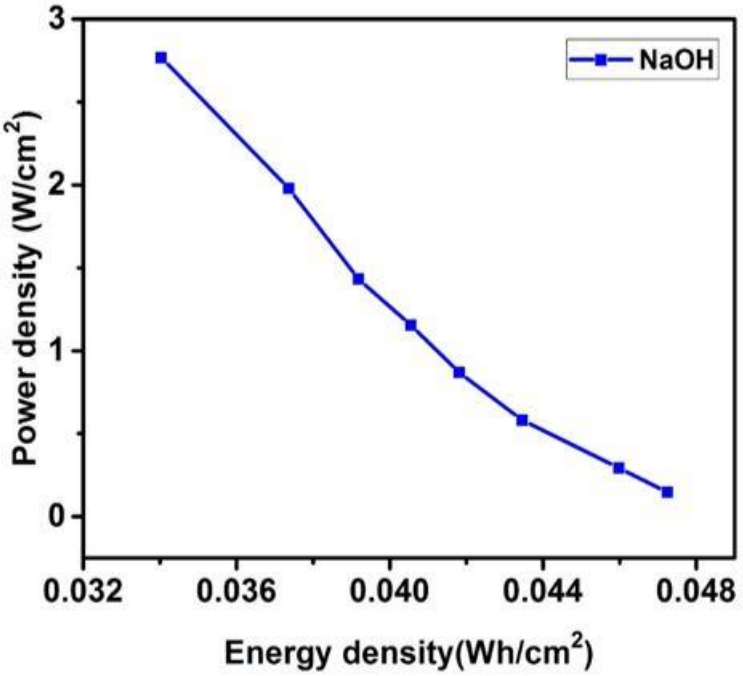

Figure 3.39: Power density versus energy density plots for Co_3O_4 in 3M NaOH electrolyte.

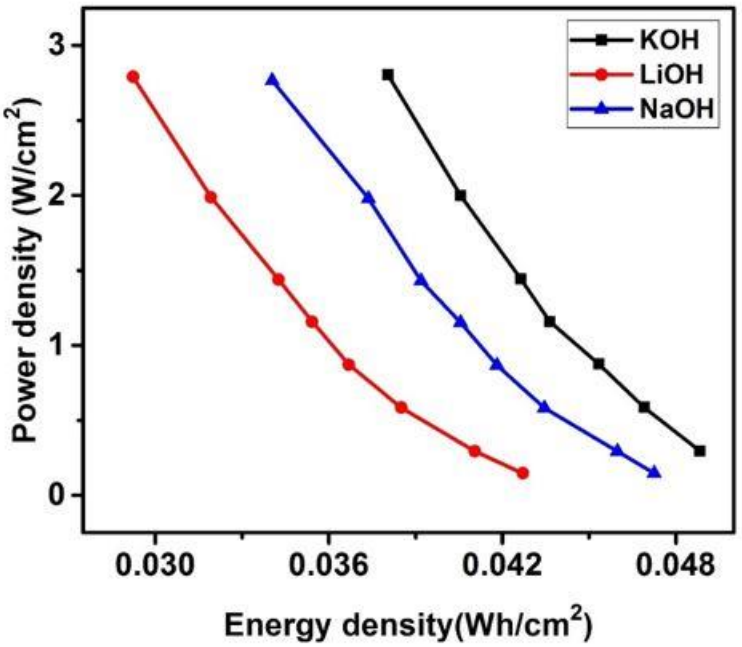

Figure 3.40: Power density versus energy density plots for Co_3O_4 in various electrolytes.

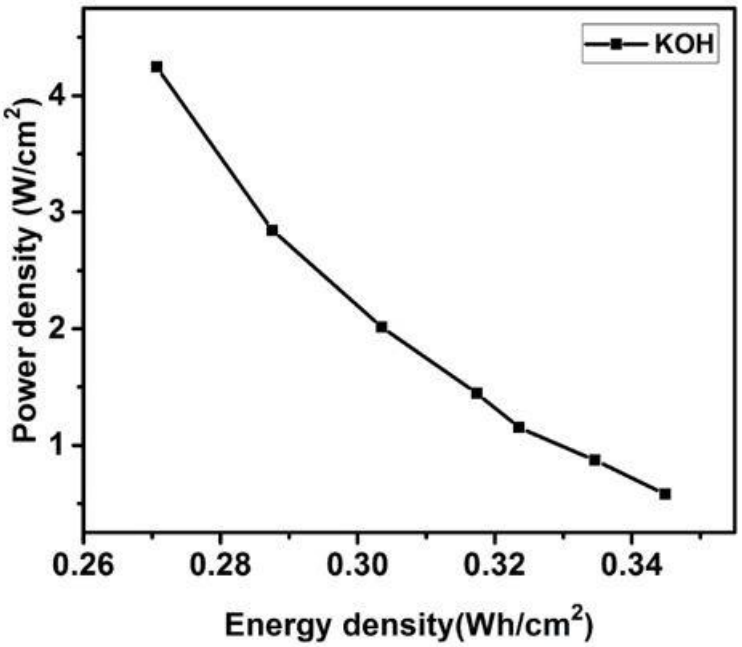

Figure 3.41: Power density versus energy density plots for Co_9S_8 in 3M KOH electrolyte.

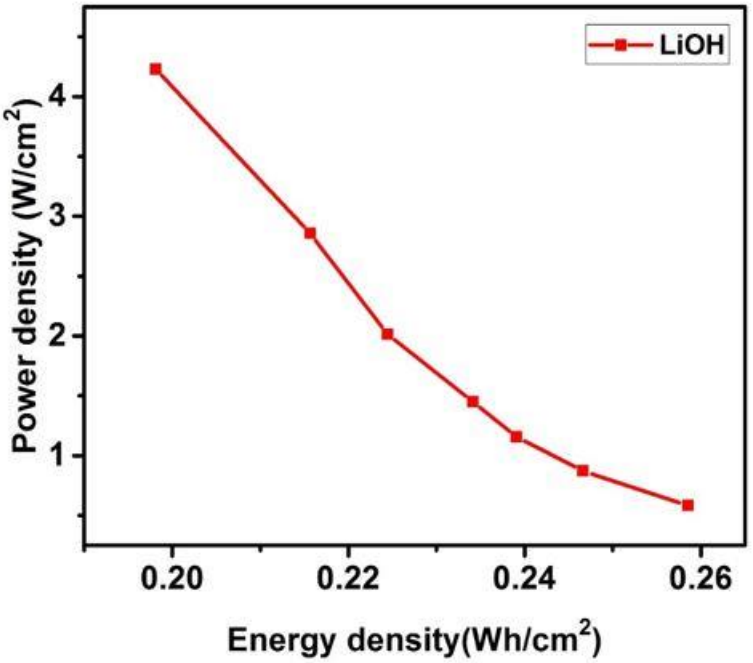

Figure 3.42: Power density versus energy density plots for Co_9S_8 in 3M LiOH electrolyte.

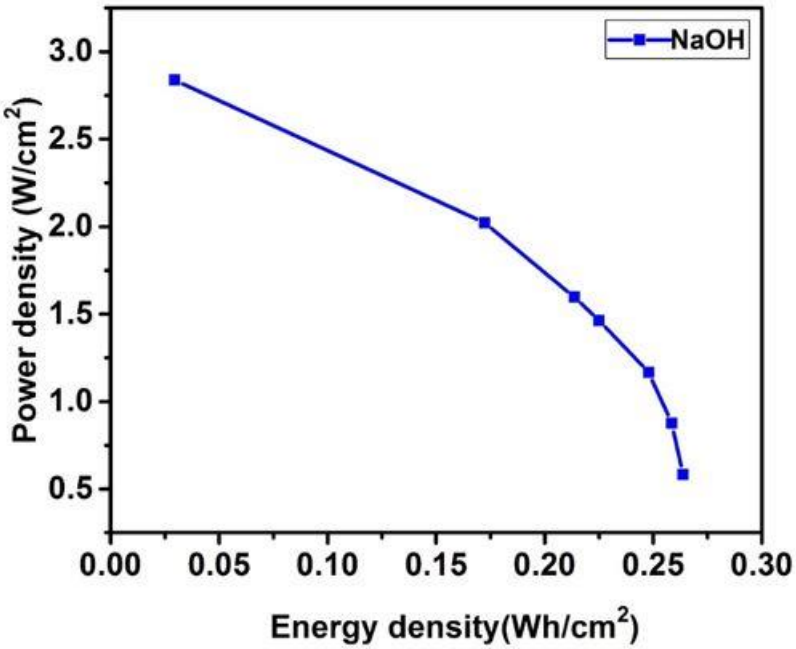

Figure 3.43: Power density versus energy density plots for Co_9S_8 in 3M NaOH electrolyte.

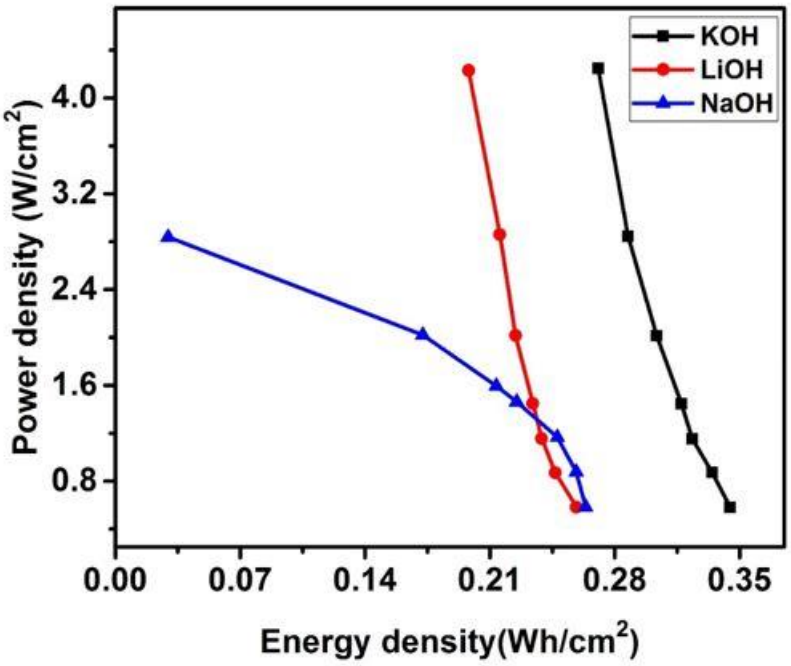

Figure 3.44: Power density versus energy density plots for Co_9S_8 in various electrolytes.

Based on cobalt oxide and cobalt sulfide electrochemical studies, the performance of Co_9S_8 electrode is higher compared to the Co_3O_4 electrode. Thus, the electrochemical properties of Co_9S_8 were tested for their application in flexible and high performance devices. Figure 3.45 shows the cyclic voltammograms of Co_9S_8 at various bending angles. As seen from the figure, the shape and size of the cyclic voltammograms of Co_9S_8 were the same at various bending angles, suggesting high flexibility and bending stability of the Co_9S_8 electrode. This study suggests that hydrothermally grown Co_9S_8 could be used as flexible electrodes for energy storage devices.

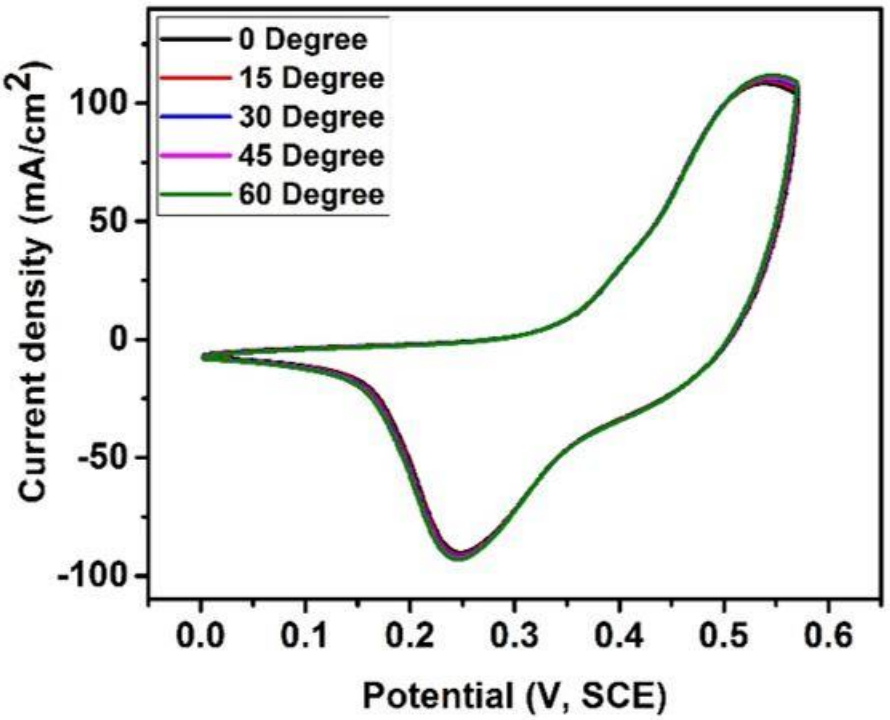

Figure 3.45: Cyclic voltammograms curves of Co_9S_8 at various bending. angles.

3.4. Electrochemical behavior of the device:

To understand the potential applicability of Co_9S_8 for flexible supercapacitor applications, the symmetrical supercapacitor device was fabricated by sandwiching an ion transporting layer between two Co_9S_8 electrodes, using 3M KOH as an electrolyte for this device. The performance of the fabricated device was studied by measuring cyclic voltammetry curves, galvanostatic charge-discharge curves under various conditions to validate its applicability, and electrochemical

impedance spectroscopy. The cyclic voltammograms of the device at room temperature at various scan rates are shown in Figure 3.46. As seen from the figure, the CV curves of the device are clearly identical in shape and are retained even at high scan rates indicating high electrochemical stability of the device. Figure 3.47 shows the specific capacitance as a function of scan rate for the supercapacitor device in 3M KOH electrolyte, showing that the specific capacitance of the device decreases with increase in scan rate which could be due to insufficient time for electrochemical reactions at the electrode.

The cyclic electrochemical stability of the supercapacitor device was examined using constant current charge-discharge method. Figure 3.48 shows the percentage of the device as the number of the cyclic studies. The device showed tremendous cyclic stability. It was observed that the percentage retention of the device first decreases up to the 1,000 th cycle and then increases with increase cyclic studies up to the 4,000 th cycle and then become almost constant. The increase in the specific capacitance of the device could be due to activation of the electrode and more complete intercalation and de-intercalation of electrolytes after the 1,000th cycle. The inset of Figure 3.48 presents the first and the 5,000th charge-discharge cycle for the device. As seen from the figure, the charge-discharge time for the 5,000th cycle is higher than that of the 1st cycle, suggesting enhancement in energy retention property. Figure 3.49 shows the electrochemical stability of the device, where the charge-discharge curves retain its shape and principally symmetrical even after a long charge-discharge (>122k s) process.

The temperature-dependent electrochemical performance of the device was investigated using cyclic voltammograms, galvanostatic charge-discharge and electrochemical impedance measurements. Figure 3.50 shows cyclic voltammograms of the device at various temperatures. The CV curves of the device indicted the near ideal capacitive nature of the fabricated device within a wide temperature window. The area under the CV curves was increased with increasing

temperature, indicating enhanced charge storage capacity of the device at high temperature. Figure 3.51 shows the effect of temperature on the charge storage capacity. As seen from the figures, the specific capacitance of the device increases with increasing temperature, showing about 100% improvement in the specific capacitance when the working temperature was increased from 10 to 70 ^{o}C. The results suggest that supercapacitor devices based on cobalt sulfides are more efficient at higher temperature. Furthermore, the charge-discharge study is shown in Figure 3.52. The discharge-time curves were observed to increase with the increasing in the temperature indicating a high storage property of the device.

Electrochemical impedance spectroscopy (EIS) was further used to analyze the temperature-dependent electrochemical behavior of the device, such as the effect of temperature on the resistive and capacitive properties. Figure 3.53 shows a decrease in the real (Z_{real}) and imaginary (Zi_{mg}) impedance with increasing device temperature. The equivalent series resistance (ESR) of the device decreases with increasing temperature, indicating the improvement of the charge storage capacity of the device. The decrease in the ESR value might be due to the enhanced mobility of the ions in the electrolyte, which increases the conductivity of the electrolyte [53]. It was further noted that the impedance of the supercapacitor decreases with increase in temperature and frequency as shown in Figure 3.54.

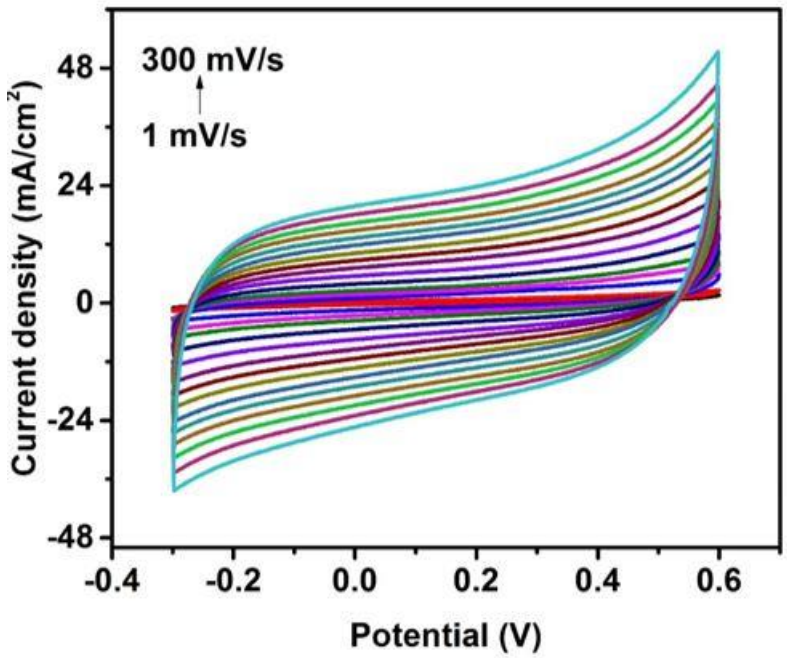

Figure 3.46: Cyclic voltammograms of the device at room temperature in various scan rates.

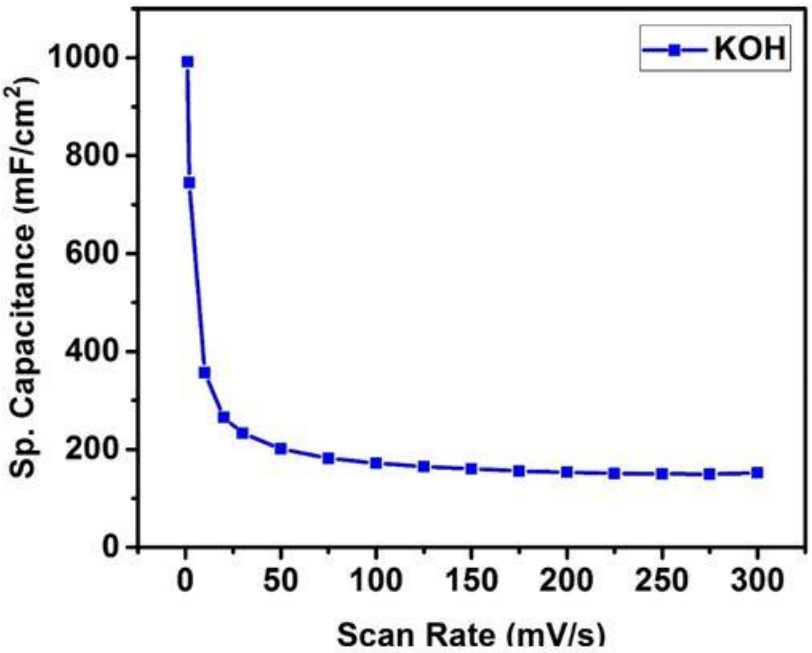

Figure 3.47: Specific capacitance as a function of scan rate for the device in 3M KOH electrolyte.

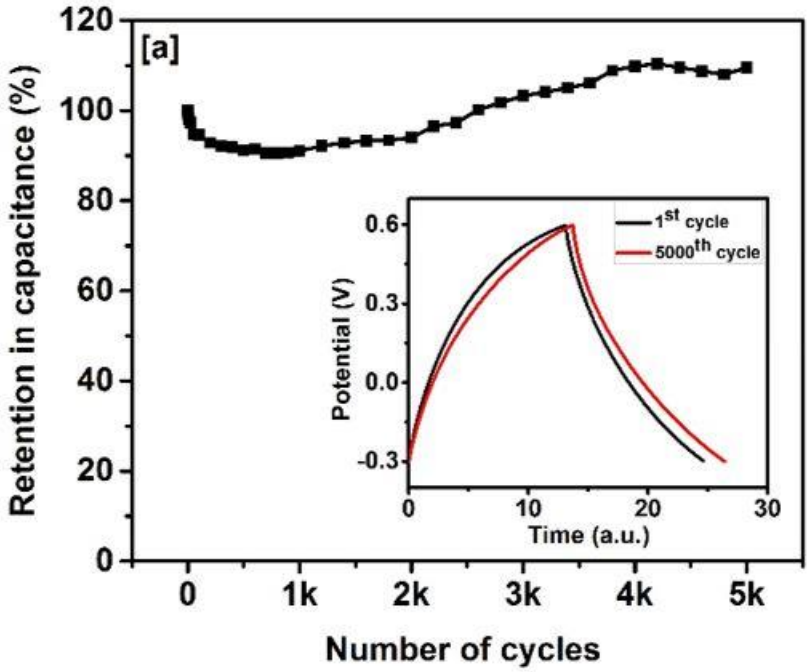

Figure 3.48: Capacitance retention versus number of charge-discharge cycles for the device based on Co_9S_8 in 3M KOH electrolyte (inset figure-potential vs. time plot for 1st and 5000th cycle of charge discharge).

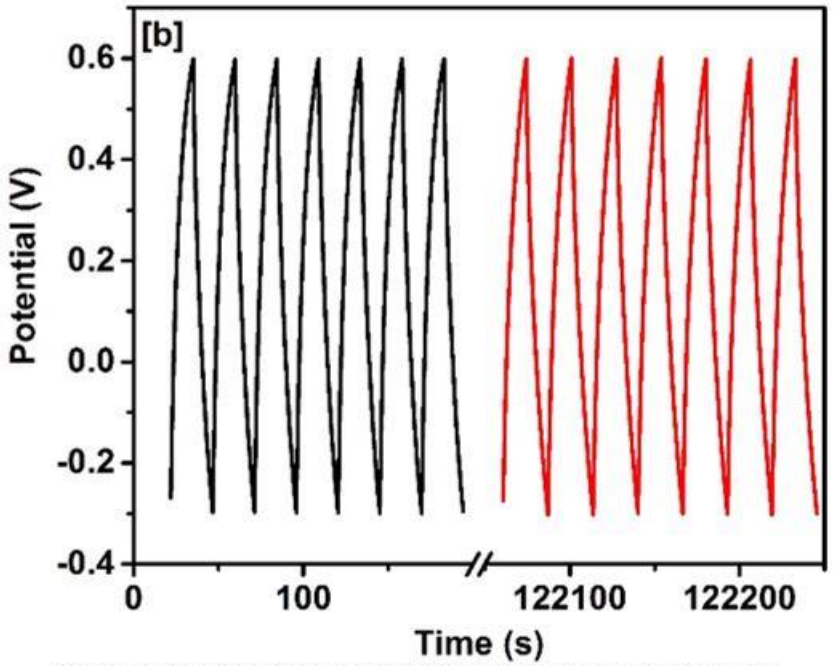

Figure 3.49: First few and last few cycles of charge discharge profile of the device.

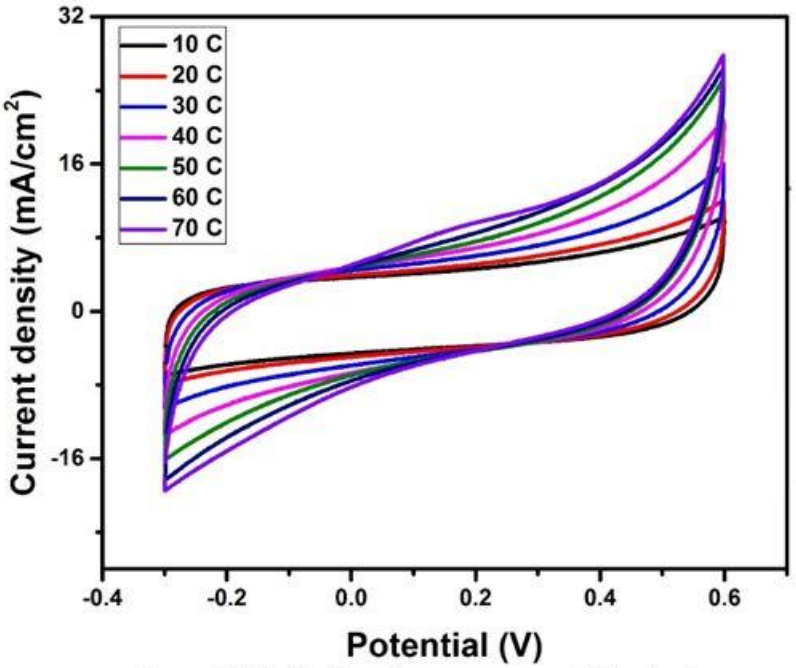

Figure 3.50: Cyclic voltammograms of the device at various temperatures.

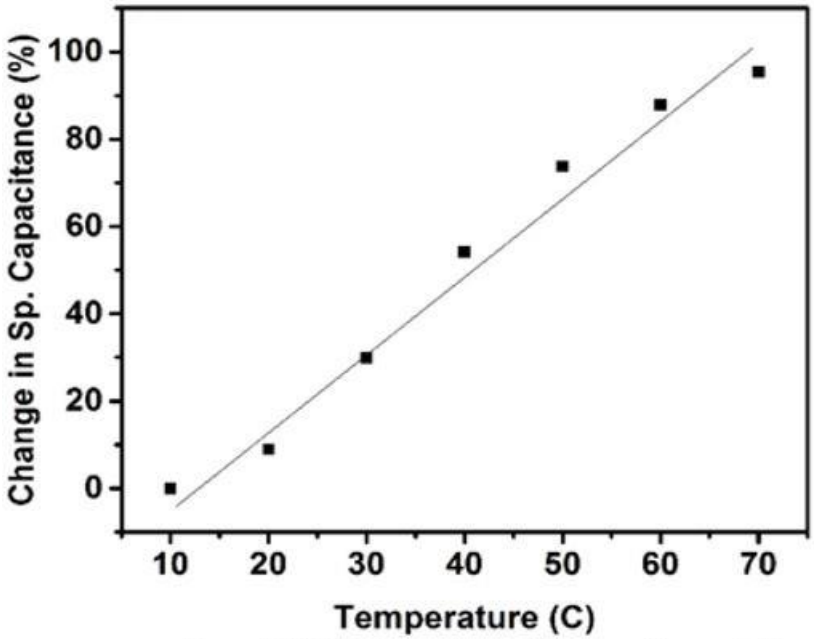

Figure 3.51: % change in specific capacitance of the device versus temperatures.

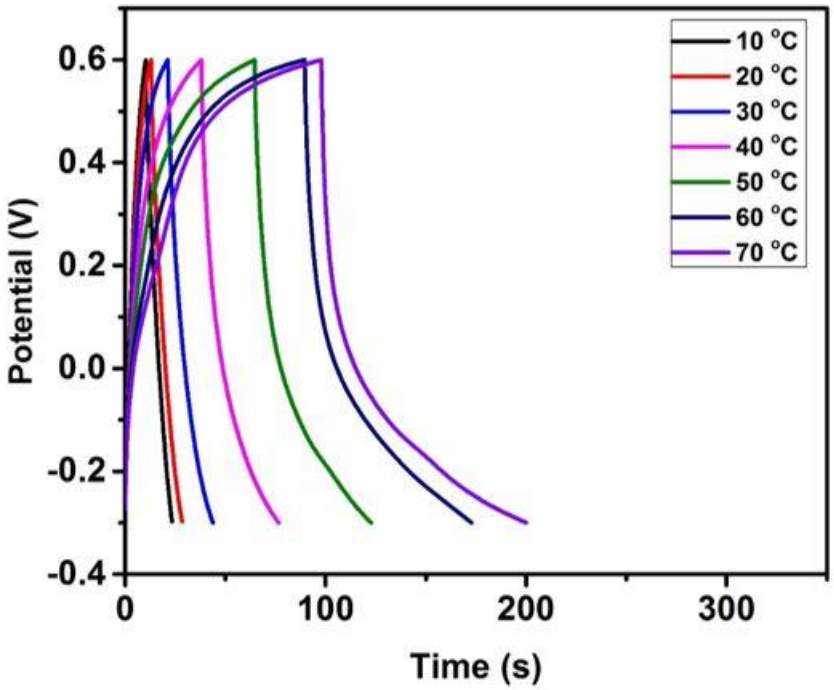

Figure 3.52: Galvanostatic charge-discharge characteristics of the device at various applied temperatures.

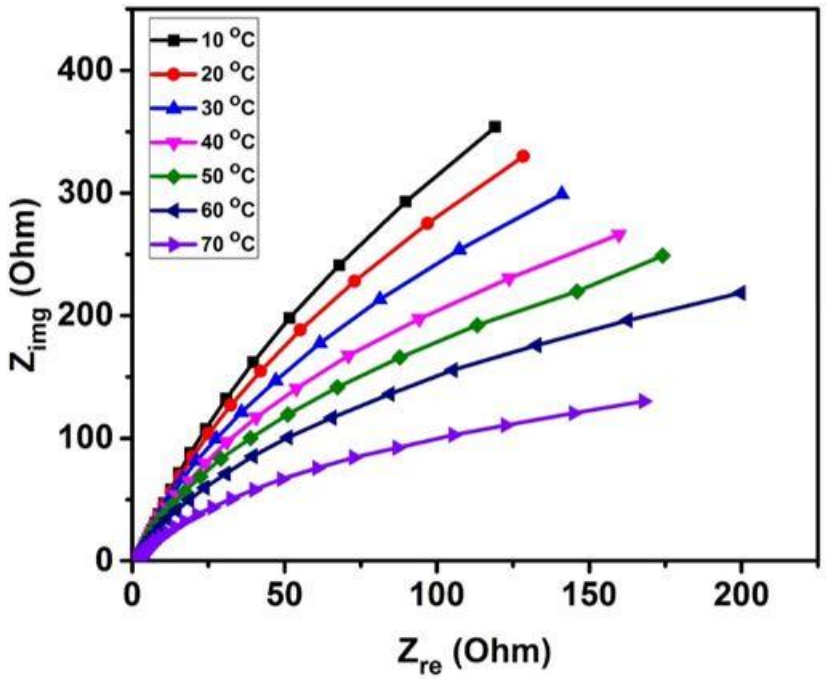

Figure 3.53: Z_{im} versus Z_{re} plots of the device at various temperatures.

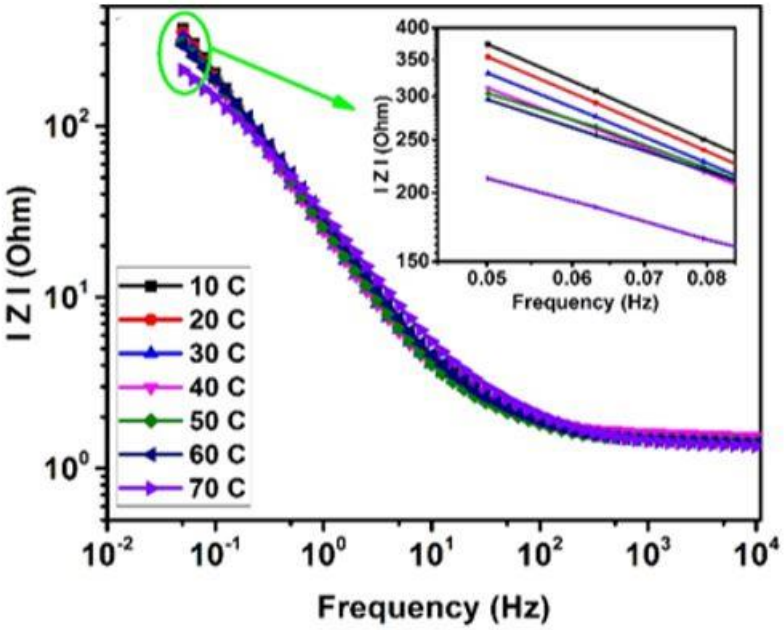

Figure 3.54: Variation of impedance as a function of frequency and temperature.

CHAPTER IV

CONCLUSION

In summary, binder free cobalt oxide transformed into cobalt sulfide nanostructures has been successfully synthesized via a facile hydrothermal technique. The obtained nanostructured cobalt oxide and cobalt sulfide has been characterized electrochemically and structurally. The structural analysis for the synthesized cobalt oxide and cobalt sulfide was conducted by employing X-ray diffraction and energy-dispersive X-ray spectrometer. The X-ray diffraction patterns of the synthesized powders showed the purity phases of cobalt oxide and cobalt sulfide. Additionally, EDX was used to confirm the cobalt oxide and cobalt sulfide formation. Scanning electron microscopy images were used to detect the surface morphology and particle size of cobalt oxide and cobalt sulfide growth on nickel foam. Electrochemical investigations have been carried out systematically preforming the effect of the electrolytes on the charge storage capacity of fabricated cobalt oxide and cobalt sulfide. All electrochemical measurements were performed in a standard three electrode cell. The cyclic voltammograms of Co_3O_4 and Co_9S_8 electrodes at low scan rates showed two sets of redox peaks indicating typical pseudocapacitive behavior. Moreover, the specific capacitance was decreased with increasing scan rate. The electrochemical properties of cobalt oxide have been improved significantly after converting to cobalt sulfide, showing specific capacitances of 983 and 7358 mF/cm^2 at 2 mA/cm^2, respectively which is over 7 times improvement in charge storage capacity. The electrochemical properties were further analyzed using galvanostatic charge-discharge measurements. The specific capacitance of both

fabricated materials electrodes was decreasing with increasing current. A cobalt sulfide based electrode showed outstanding flexibility without compromising its energy storage properties. Symmetrical supercapacitor device was fabricated by sandwiching an ion transporting layer between two Co_8S_9 electrodes. The performance of the device was evaluated at room temperature and elevated temperatures using cyclic voltammetry and galvanostatic charge-discharge. Cyclic voltammetry curves were increased when the temperature was increased, suggesting improvement in the charge storage capacity of the device. The device showed outstanding stability for 5,000 of cyclic study. Temperature has a drastic effect on the charge storage capacity. The device showed 100% enhancement in specific capacitance on increasing temperature 10 to 70^oC. Our results suggest that cobalt sulfide could be used as appropriate electrode material for high performance energy storage devices which could be operated effectively at elevated temperatures.

REFERENCES

1. Bagher, A. M.; Vahid, M. M.; Mohsen, M. Types of Solar Cells and Application. *Amer. J. Opt. Photonics*. **2015,** *3*, 94-113.
2. Elbatran, A. H.; Abdel-Hamed, M. W.; Yaakob, O. B.; Ahmed, Y. M.; Arif Ismail, M. Hydro Power and Turbine Systems Reviews. *Jurnal Teknologi*. **2015**, *74*, 83–90.
3. Thresher, R.; Robinson, M.; Veers, P. In Proceedings of the Physics of Sustainable Energy Conference, Berkeley, CA, March 1-2, 2008; National Renewable Energy Laboratory: Golden, CO, 2008.
4. Kim, B.; Sy, S.; Yu, A.; Zhang, J. Electrochemical Supercapacitors for Energy Storage and Conversion. *Handbook of Clean Energy Systems*, **2015**, 1–25.
5. Signorelli, R.; Ku, D.C.; Kassakian, J.G.; Schindall, J.E. Electrochemical Double-Layer Capacitors Using Carbon Nanotube Electrode Structures. *Proc. IEEE.* **2009**, *97*, 1837-1847.
6. Chen, J.; Cheng, F. Combination of Lightweight Elements and Nanostructured Materials for Batteries. *Acc. Chem. Res.* **2009**, *42*, 713-723.
7. Yong, P.L. Pacific A Level Physics; EPB Pan Pacific: Singapore, 2006; 304.
8. Simon, P.; Burke, A. Nanostructured Carbons: Double-Layer Capacitance and More. *Electrochem. Soc. Interface.* **2008,** *17*, 38–43.
9. Frackowiak, E.; Beguin, F. Electrochemical Storage of Energy in Carbon Nanotubes and Nanostructured Carbons. *Carbon*. **2002**, *40*, 1775-1787.
10. Bryan, A. M.; Santino, L. M.; Lu, Y.; Acharya, S.; D'Arcy, J. Conducting Polymers for Pseudocapacitive Energy Storage. *Chem. Mater.* **2016**, *28*, 5989-5998.
11. Mitchell, E.; De Souza, F.; Gupta, R.K.; Kahol, P.K.; Kumar, D.; Dong, L.; Gupta, B.K. Probing on the Hydrothermally Synthesized Iron Oxide Nanoparticles for Ultra-Capacitor Applications, *Powder Technol*. **2015**, *272*, 295-299.

12. Deshpande, R. P. *Ultracapacitors*. McGraw Hill Professional: New York, 2016; 346.
13. Patake, V. D.; Lokhande, C. D.; Joo, O. S. Electrodeposited Ruthenium Oxide Thin Films for Supercapacitor: Effect of Surface Treatments. *Appl. Surf. Sci.* **2009**, *255*, 4192–4196.
14. Guan D.; Gao Z.; Yang W.; Wang J.; Yuan Y.; Wang B.; Zhang M.; Liu L. Hydrothermal Synthesis of Carbon Nanotube/Cubic Fe_3O_4 Nanocomposite for Enhanced Performance Supercapacitor Electrode Material, *Mater. Sci. Eng*. **2013**, *178*, 736-743.
15. Mishra A.K.; Ramaprabhu S. Functionalized Graphene-Based Nanocomposites for Supercapacitor Application, *J. Phys. Chem.* **2011,** 115, 14006-14013.
16. Wang Q.; Jiao L.; Du H.; Wang Y.; Yuan H. Fe_3O_4 Nanoparticles Grown on Graphene as Advanced Electrode Materials for Supercapacitors. *J. Power Sources*. **2014**, *245*, 101-106.
17. Kim, B.; Sy, S.; Yu, A.; Zhang, J. Electrochemical Supercapacitors for Energy Storage and Conversion. *Handbook of Clean Energy Systems*, **2015**, 1–25.
18. Malak, A.; Fic, K.; Lota, G.; Vix-Guterl, C.; Frackowiak, E. Hybrid Materials for Supercapacitor Application*. J. Solid State Electrochem*. **2010**, *14*, 811–816.
19. Wu, Z.S.; Ren, W.C.; Wang, D.W.; Wang, D.W.; Li, F.; Liu, B.; Cheng, H.M. High-energy MnO_2 Nanowire/Graphene and Graphene Asymmetric Electrochemical Capacitors. *ACS Nano*, **2010**, *4*, 5835–5842.
20. Fan, Z.; Yan, J.; Wei, T.; Zhi, L.; Ning, G.; Li, T.; Wei, F. Asymmetric Supercapacitors Based on Graphene/MnO_2 and Activated Carbon Nanofiber Electrodes with High Power and Energy Density. *Adv. Funct. Mater.* **2011**, *21*, 2366–2375.
21. Electric Double Layer Capacitor. http://nuintek.tradekorea.com (accessed Oct 13, 2004).
22. Zou, R.; Yuen, M. F.; Yu, L., Hu, J.; Lee, C.; Zhang, W. Electrochemical Energy Storage Application and Degradation Analysis of Carbon-Coated Hierarchical $NiCo_2S_4$ Core-Shell Nanowire Arrays Grown Directly on Graphene / Nickel Foam. *Sci. Rep.* **2015**, *6*, 1–9.

23. Jiang, J.; Li, Y.; Huang, X.; Yuan, c. Recent Advances in Metal Oxide-based Electrode Architecture Design for Electrochemical Energy Storage. *Materials*. **2012**, *24*, 5166-5180.

24. Shin, C.; Manuel, J.; Kim, D.; Ryu, H.A.; Ahn, J. Structural Characterization and Electrochemical Properties of Co_3O_4 Anode Materials Synthesized by a Hydrothermal Method. *Nanoscale Res. Lett.* **2012**, *7*, 1-7.

25. Qiu, H.; Liu, L.; Mu, Y.; Zhang, H.; Wang, Y. Designed Synthesis of Cobalt-Oxide-Based Nanomaterials for Superior Electrochemical Energy Storage Devices. *Nano Res.* **2014.**

26. Maruyama, T.; Arai, S. Electrochromic Properties of Cobalt Oxide Thin Films Prepared by Chemical Vapor Deposition. *J Electrochem Soc.* **1996**, *143*, 1383–1386

27. Schmidtszalowski, K; Krawczyk, K.; Petryk, J. The Properties of Cobalt Oxide Catalyst for Ammonia Oxidation. *Appl. Catal., A.* **1998**, *175*, 147–157.

28. Yang, Y. F.; Sangeetha, P.; Chen, Y.W. Au/TiO_2 Catalysts Prepared by Photo-Deposition Method for Selective CO Oxidation in H_2 Stream. *International Journal of Hydrogen Energy*, **2009**, *34*, 8912–8920.

29. Huang, T. J.; Tsai, D. H. CO Oxidation Behavior of Copper and Copper Oxides, *Catalysis Letters*, **2003**, *87*, 173–178.

30. Manteghi, F.; Kazemi, S. H.; Peyvandipour, M.;Asghari, A. Preparation and Application of Cobalt Oxide Nanostructures as Electrode Materials for Electrochemical Supercapacitors. *RSC Adv.* **2015**, *5*, 76458–76463.

31. Dar, F. I.; Moonoosawmy, K. R.; Es-Souni, M. Morphology and Property Control of NiO Nanostructures for Supercapacitor Applications. *Nanoscale Res. Lett.*, **2013**, *8*, 363.

32. Lu, Z.; Chang, Z.; Liu, J; Sun, X. Stable Ultrahigh Specific Capacitance of NiO Nanorod Arrays. *Nano Res*. **2011**, *4*, 658.

33. Marco, J.; Gancedo, J.R.; Gracia, M.; Gautier, J.L.; Rıos, E.; Berry, F.J. Characterization of the Nickel Cobaltite, $NiCo_2O_4$, Prepared by Several Methods: An XRD, XANES, EXAFS, and XPS Study. *J. Solid State Chem.* **2000**, *153*, 74–81.

34. Hussain, M.; Ibupoto, Z.H.; Abbasi, M.A.; Liu, X.; Willander, M. Synthesis of Three Dimensional Nickel Cobalt Oxide Nanoneedles on Nickel Foam, Their Characterization and Glucose Sensing Application. *Sensors*, **2014**, *14*, 5415–5425.

35. Wu, Z.; Zhu, Y.; Ji, X. $NiCo_2O_4$ based Materials for Electrochemical Supercapacitors. *J. of Mater. Chem. A*. **2014**, *2*, 14759–14772.

36. Chen, Y.; Qu, B.; Hu, L.; Xu, Z.; Li, Q.; Wang, T. High-Performance Supercapacitor and Lithium-Ion Battery Based on 3D Hierarchical NH_4F-Induced Nickel Cobaltate Nanosheet-Nanowire Cluster Arrays as Self-Supported Electrodes. *Nanoscale*. **2013**, *5*, 9812-9820.

37. Zou, R.; Xu, K.; Wang, T.; He, G.; Liu, Q.; Liu, X.; Zhang, Z.; Hy, J. Chain-Like $NiCo_2O_4$ Nanowires with Different Exposed Reactor Planes for High-Performance Supercapacitors. *J. Mater. Chem. A.* **2013**, *1*, 8560-8566.

38. Rui , X. H.; Tan, H. T.; Yan, Q. Y. Nanostructured Metal Sulfides for Energy Storage. *Nanoscale* **2014** , *6*, 9889-9924.

39. Huang, X.; Zeng, Z. Y.; Zhang, H. Metal Dichalcogenide Nanosheets: Preparation, Properties and Applications. *Chem. Soc. Rev.* **2013** , *42*, 1934-1946.

40. Wang, Q.; Jiao, L.; Du, H.; Yang, J.; Huan, Q.; Peng, W.; Si, Y.; Wang, Y.; Yuan, H. Facile Synthesis and Superior Supercapacitor Performances of Three-Dimensional Cobalt Sulfide Hierarchitecture. *CrystEngComm*. **2011**, *13*, 6960-6963.

41. Yang, Z.; Chen, C. Y.; Chang, H. T. Supercapacitors Incorporating Hollow Cobalt Sulfide Hexagonal Nanosheets. *J. Power Sources.* **2011**, *196*, 7874-7877.

42. Yang, J.; Duan, X.; Qin, Q.; Zheng, W. Solvothermal Synthesis of Hierarchical Flower-Like Beta-NiS with Excellent Electrochemical Performance for Supercapacitors. *J. Mater. Chem., A.* **2013**, *1*, 7880-7884.

43. Huang, G.; Chen, T.; Wang, Z.; Chang, K.; Chen, W. Synthesis and Electrochemical Performances of Cobalt Sulfides/Graphene Nanocomposite as Anode Material of Li-Ion Battery, *J. Power Sources*, **2013**, *235*, 122-128.

44. Chen, H.; Kung, C.; Tseng, C.; Wei, T.; Sakai, N.; Morita, S.; Ikegama, M.; Miyasaki, T.; Ho, K. Plastic Based Dye-Sensitized Solar Cells Using Co_9S_8 Acicular Nanotube Arrays as the Counter Electrode. *J. Mater. Chem., A*. **2013**, *1*, 13759-13768.

45. Hu, Q. R.; Wang, S. L.; Zhang, Y.; Tang, W. H. Synthesis of Cobalt Sulfide Nanostructures by a Facile Solvothermal Growth Process. *J. Alloys Compd.* **2010**, *491*, 707–711.

46. Wang, Q.; Jiao, L.; Du, H.; Peng, W.; Han, Y.; Song, D.; Si, Y.; Wang, Y.; Yuan, H. Novel Flower-Like CoS Hierarchitectures: One-Pot Synthesis and Electrochemical Properties. *J. Mater. Chem.* **2011**, *21*, 327-329.

47. Meng, X.; Deng, J.; Zhu, J.; Bi, H.; Kan, E.; Wang, X. Cobalt Sulfide/Graphene Composite Hydrogel as Electrode for High-Performance Pseudocapacitors. *Sci. Rep.* **2016**, *6*, 21717.

48. Gu, Y.; Xu, Y.; Wang, Y. Graphene-Wrapped CoS Nanoparticles for High-Capacity Lithium-Ion Storage. *ACS Appl. Mater. Interfaces*. **2013**, *5*, 801–806.

49. Pu, J.; Wang, Z.; Wu, K.; Yu, N.; Sheng, E. Co_9S_8 Nanotube Arrays Supported on Nickel Foam for High-Performance Supercapacitors. ***Phys. Chem. Chem. Phys.*** **2014**, ***16***, 785-791.

50. Jana, M.; Saha, S.; Samanta, P.; Murmu, N. C.; Kim, N. H.; Kuila, T.; Lee, J. H. Development of High Energy Density Supercapacitor through Hydrothermal Synthesis of RGO/Nano-Structured Cobalt Sulphide Composites. *Nanotechnology* **2015**, *26*, 075402/1-075402/14.

51. Zhang, Y.; Wang, Q. The New Process of Nickel Sulfide Synthesis. *Adv. Mater. Res*. **2012**, *366*, 318.

52. Denholme, S.J.; Gallagher, J.B.; Dobson, P.S.; Weaver, J.M.; Gregory, D.H. *Isr. J. Chem*. **2010**, *50*, 515.

53. Fazli, Y.; Mahdi Pourmortazavi, S.; Kohsari, I.; Sadeghpur, M. Electrochemical Synthesis and Structure Characterization of Nickel Sulfide Nanoparticles. *Mater. Sci. Semicond. Process.* **2014**, *27*, 362–367.

54. Pan, Q.; Huang, K.; Ni, S.; Yang, F.; He, D. Synthesis of Flower- and Rod-Like Nickel Sulfide Nanostructures by an Organic-Free Hydrothermal Process. *Mater. Res. Bull.* **2008**, *43*, 1440–1447.

55. Gaikar, P.; Pawar, S. P.; Mane, R. M.; Muashad, M.; Shinde, D. V. Synthesis of Nickel Sulfide as a Promising Electrode Material for Pseudocapacitor. ***RSC Adv.*** **2016**, ***6***, 112589-112593.

56. Li, D.; Gong, Y.; Pan, C. Facile Synthesis of Hybrid CNTs/$NiCo_2S_4$ Composite for High Performance Supercapacitors. *Sci. Rep*. **2016**, *6*, 29788.

57. Chen, H. C.; Jiang, J.; Zhang, L.; Wan, H.; Qi, T. *Highly Conductive $NiCo_2S_4$ Urchin-Like Nanostructures for High-Rate Pseudocapacitors. Nanoscale* **2013**, *5,* 8879–8883.

58. Park, S. H.; Sun, Y.; Park, K. S.; Nahm, K. S.; Lee, Y. S.; Yoshio, M. *Synthesis and Electrochemical Properties of Lithium Nickel Oxysulfide ($LiNiS_yO_{2-y}$) Material for Lithium Secondary Batteries*. *Electrochim. Acta.* **2002**, *47*, 1721–1726.

59. Liu, Y.; Zhang, J.; Wang, S.; Wang, K.; Chen, Z.; Xu, Q. *Facilely Constructing 3D Porous $NiCo_2S_4$ Nanonetworks for High-Performance Supercapacitors*. *New J. Chem.* **2014**, *38*, 4045–4048.

60. Yang, J.; Ma, M.; Sun, C.; Zhang, Y.; Huang, W.; Dong, X. *Hybrid $NiCo_2S_4$@MnO_2 Heterostructures for High-Performance Supercapacitor Electrodes*, *J. Mater. Chem. A* **2015**, *3*, 1258–1264.

61. H. Zhang, S.C. Wang, D. Xue, Q. Chen, Z.C. Li, Preparation of Nanocrystalline CeO_2 by Nanocasting with Mesoporous Silica. *Journal of Physics*: Conference Series, **2009**, *152*, 012070.

62. Gomez, J.; Kalu, E. E. High-Performance Binder-Free Co–Mn Composite Oxide Supercapacitor Electrode. *J. Power Sources*, **2013**, *230*, 218-224.

63. Xie, L. J.; Wu, J. F.; Chen, C. M.; Zhang, C. M.; Wan, L.; Wang, J. L.; Kong, Q. Q.; Lv, C.X.; Li, K. X.; Sun, G. H. A Novel Asymmetric Supercapacitor with an Activated Carbon Cathode and a Reduced Graphene Oxide–Cobalt Oxide Nanocomposite Anode. *J. Power Sources*, **2013**, *242*,148-156.

64. Mujawar, S. H.; Ambade, S.B.; Battumur, T.; Ambade, R.B.; Lee, S.-H. Electropolymerization of Polyaniline on Titanium Oxide Nanotubes for Supercapacitor Application, *Electrochim. Acta*, **2011**, *56* ,4462-4466.

65. Li, W.; Xu, K.; An, L.; Jiang, F.; Zhou, X.; Yang, J.; Chen, Z.; Zou, R.; Hu, J. Effect of Temperature on the Performance of Ultrafine MnO_2 Nanobelt Supercapacitors*. J. Mater. Chem., A* **2014**, *2*, 1443-1447.

66. Tummala R.; Guduru R. K.; Mohanty P. S. Nanostructured Co_3O_4 Electrodes for Supercapacitor Applications from Plasma Spray Technique. *J. Power Sources* 2012, *209*, 44–51.

67. Li, H. Gao, Y.; Shao, Y.; Su, Y.; Wang, X. Vapor-Phase Atomic Layer Deposition of Co_9S_8 and Its Application for Supercapacitors. *Nano Lett.* **2015**, *15*, 6689-6695.